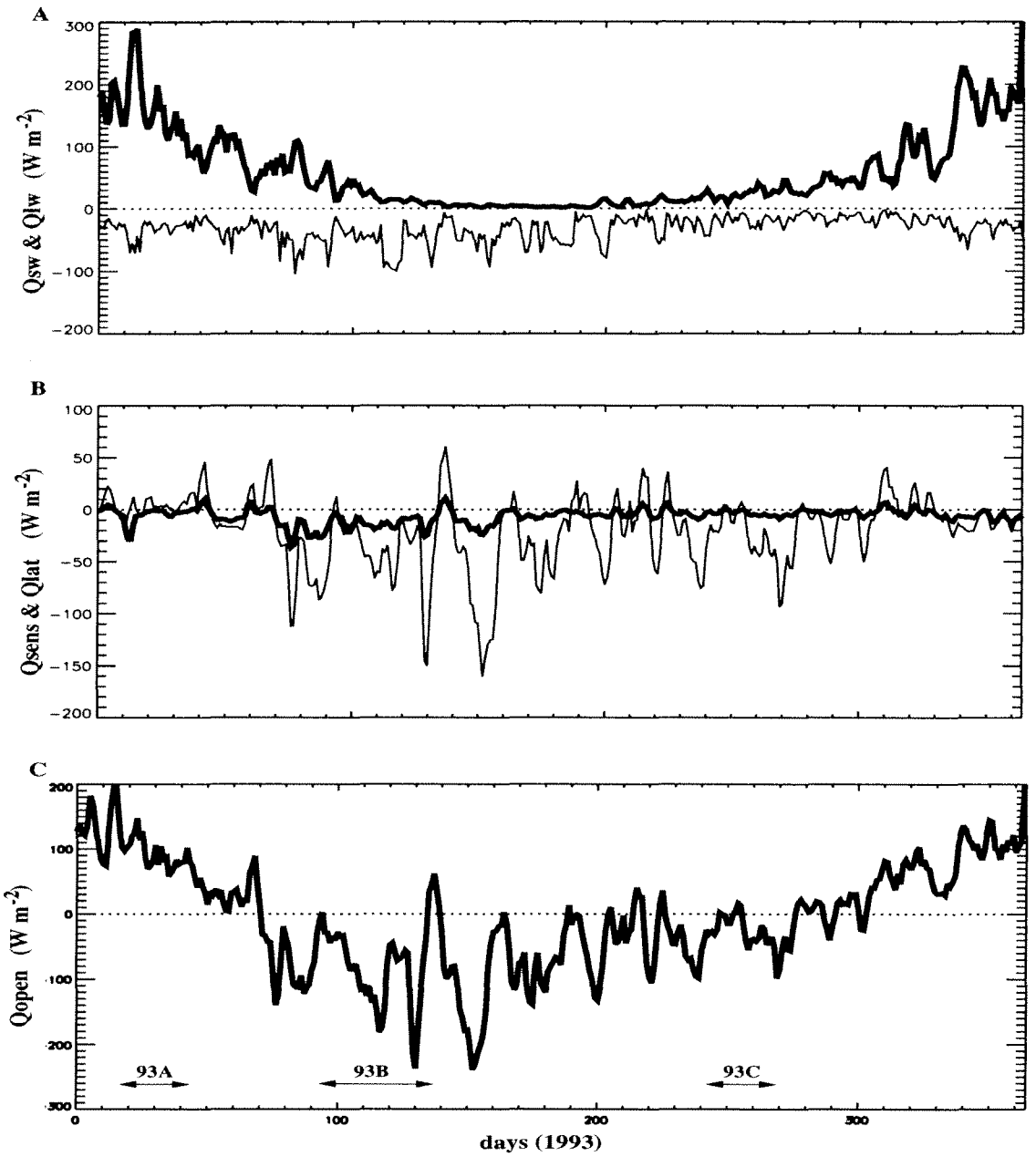

Figure 18. Ice free, surface heat budget calculated for 1993. Positive heat fluxes indicating AASW surface warming. All values are multiplied by (1 - A_i) (see Equation 8) and smoothed with a 3-day filter for presentation. A) (1 -α_s)· Q_{sw} (thick line) and $\epsilon \cdot (Q_{lw}^{back} - Q_{lw}^{down})$ (thin line). B) Q_{lat} (thick line) and Q_{sens} (thin line). C) Total Q_{open} from Equation 8. The x-axis is in days since January 1, 1993. The beginning and ending dates of the cruises to the region during the summer (93A), fall (93B) and winter (93C) are indicated by arrows and zero heat flux is indicated with a horizontal dotted line for reference.

only a few degrees resulting in sensible heat exchanges which averages near zero and ranges between ± 5 to 10 W m^{-2} (Figure 18b). Large temperature differences between the ocean and the atmosphere during the late fall, and winter, cause large sensible heat losses which can exceed 100 to 150 W m^{-2} (Figure 18b). The contribution of latent heat loss (Q_{lat}) to the ice free heat budget is usually insignificant compared to sensible contributions, being typically 4 to 10 times smaller (Figure 18b and Table 3). The low values for latent heat exchanges are typical for maritime environments and result from high relative humidity (Figure 16c) which suppresses evaporation. Daily averaged humidity at Faraday is 80 to 90% while relative humidities between 95 and 100% were recorded during the March to May 1993 (93B) cruise [Smith et al., 1993a].

The summer heat budget is dominated by surface heating from short wave radiation while the winter budget has large sensible heat losses through ice-free leads. Sensible heat losses through leads are episodic and reflect fluctuations in the atmospheric temperature (Figure 16b). The largest sensible heat losses (i.e. 100 to 150 W m^{-2}) typically occur when light to moderate winds (i.e. 2 to 5 m s^{-1}) are out from the south with cold atmospheric conditions (Figure 17). These significant sensible heat losses during the winter combine with the persistent heat loss from long wave radiation to force overall ice-free heat budget (Q_{open}) to cool the surface with losses on the order of 150 to 200 W m^{-2}.

Occasional mid-winter, warm atmospheric conditions (e.g., days 135 and 210-220 in Figure 18c) can change sensible heat exchanges from winter maximum heat losses to near zero values. On occasion, sensible heat exchanges are positive causing surface AASW warming during the winter.

The approach used to obtain daily values of SST (Section 3.1.3) introduces uncertainty into the ice free heat budget (Q_{open}). To evaluate the sensitivity of the calculation to SST, the heat budget was recalculated with SST=0°C (Q'_{open}). Other

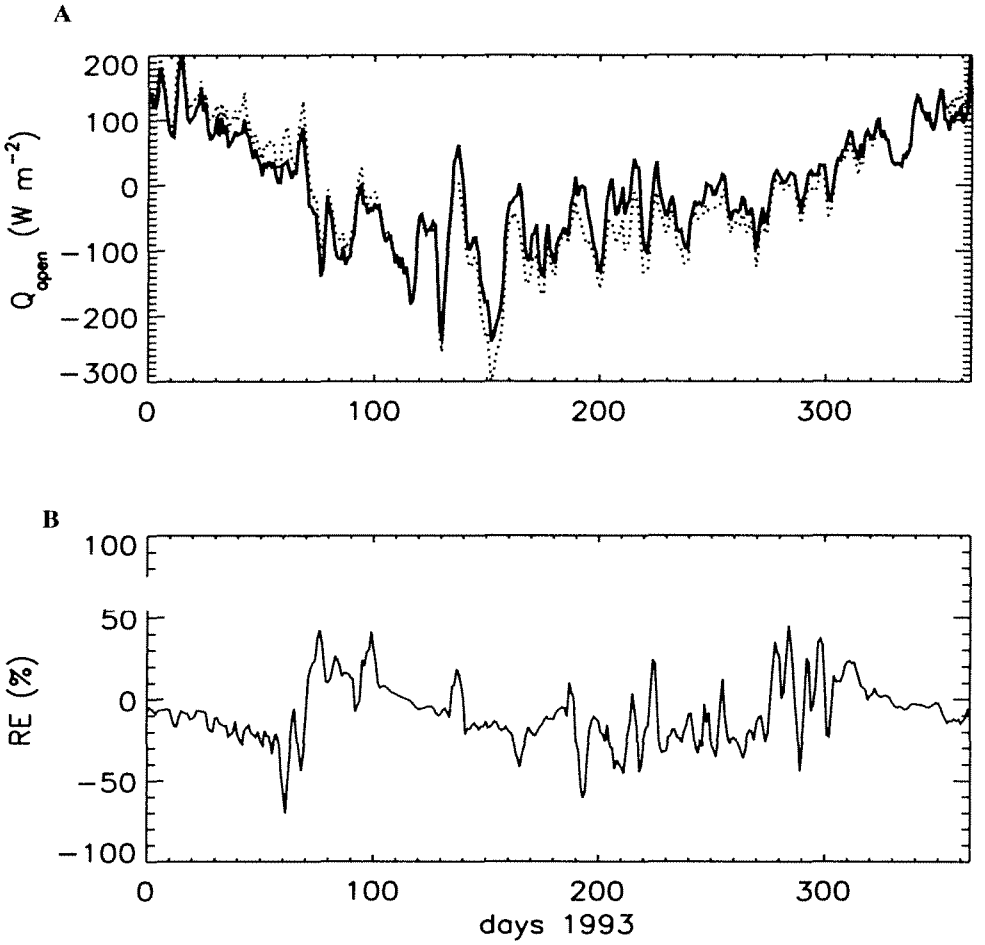

Figure 19. Sensitivity of the open ocean heat budget to SST. A) Heat budget for ice free conditions calculated using derived SST time series (Q_{open}) (thick line) and calculated with SST=0 (Q'_{open}) (thin line). B) Relative error (RE) between Q_{open} and Q'_{open} with RE = (Q_{open} - Q'_{open}) / (*smooth* Q_{open}) where *smooth* indicates the use of a 3 day smoother. The average RE is approximately -5%.

choices for SST between -2 and 2 °C yield quantitatively similar results when recalculating the budget (analysis not shown). The average relative error (RE) between the ice-free budget and the ice-free budget with SST=0 (Figure 19b), is approximately -12% with the largest errors resulting during the fall and winter when sensible heating is important in the ice-free heat budget. This average is artificially inflated by a few days when the calculated ice-free budget is near zero and small variations between the two calculations result in fairly large percentages.

During late-spring through early-fall, short wave radiation dominates the budget and errors due to the choice of SST are minimal because SST primarily enters the calculation through sensible heat fluxes in the fall through winter months. As the dominance of short wave heating diminishes in the fall, the temperature difference between the atmosphere and the ocean increases, ($\Delta_{air-\mathrm{SST}} \simeq 15°\mathrm{C}$) and the contribution of SST to the overall heat budget through sensible heating increases. This winter temperature difference between the atmosphere and ocean is largely determined by changes in the atmospheric temperature as SST remains close to the freezing point. Thus variations in the winter sensible heat exchanges are coincident with variations in the atmospheric conditions.

4.1.3 Heat and salt flux through the permanent pycnocline

As discussed in Section 3.2.2, the presence of warm, salty water of oceanic origin on the shelf provides a reservoir of heat and salt that can be transfered across the permanent pycnocline into the AASW layer.

A necessary condition for the double diffusive instability is Turner Angle (Tu) $< 45°$ [Kelly, 1984]. A sample vertical distribution of temperature and salinity for the 600.140 station (Figure 20a) illustrates the double diffusive calculation using the MC76 model (Figures 20b-c). The permanent pycnocline for 600.140 is characterized by Tu on the order of -65 to -50° (Figure 20b), which results in a maximum double

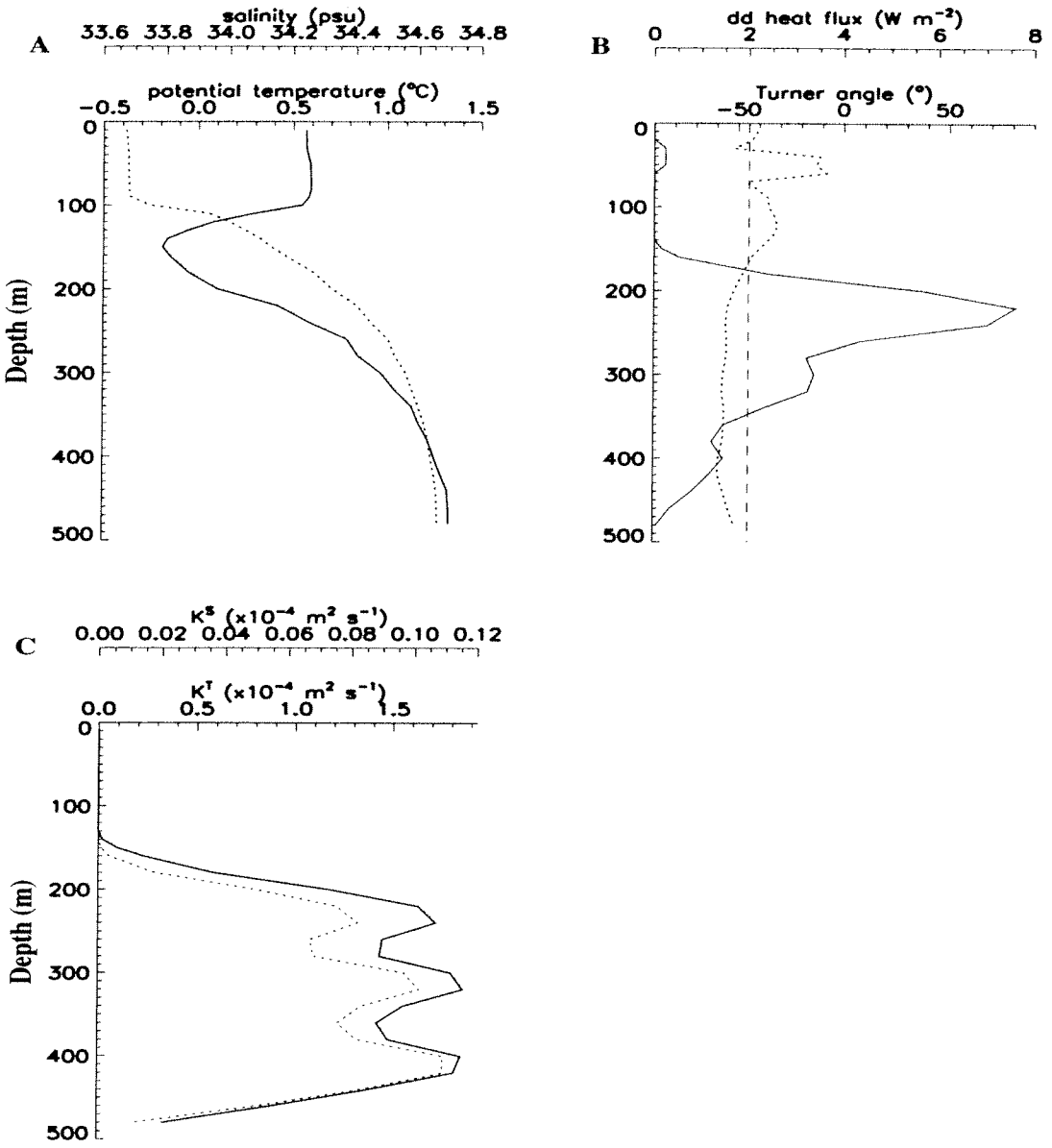

Figure 20. Double diffusive heat flux calculation for station 600.140 (Fall 1993). Vertical distributions of A) temperature and salinity at station 600.140 observed in March-May 1993, B) calculated Turner angle (dotted line) and the double diffusive heat flux (solid line) and C) mixing coefficients associated with the double diffusive heat and salt fluxes.

diffusive heat flux of 8 W m^{-2} at a mid-pycnocline depth of 210 m, the depth of the maximum of temperature and salinity gradients (Figure 20a,b).

Double diffusive mixing coefficients associated with the maximum double diffusive heat flux are found using (15) and (16) as K_{dd}^{T}=1.5×10^{-4} and K_{dd}^{S} = 1.2×10^{-5} m^2 s^{-1}, respectively (Figure 20c). The order of magnitude difference between K_{dd}^{T} and K_{dd}^{S} is typical of double diffusive regimes with $R_\rho > 2$ ($Tu <$ -50°C) (Figure 10). The box model calculations presented in Smith et al. [1999] and Klinck [1998] required different vertical mixing coefficients to balance onshore fluxes of heat and salt in order to maintain the observed hydrographic structure of the sub-pycnocline waters.

The across-shelf distribution of double diffusive heat flux, calculated using the MC76 model and temperature and salinity data collected during the 1993 fall cruise across the 600 line, is fairly uniform with maximum values around 10 W m^{-2} (Figure 21). The fluxes are found at depths associated with the permanent pycnocline and tens of meters below WW (sub-surface temperature minimum in Figure 20). The only significant structure in the across-shelf distribution occurs at the shelf break boundary between modified-UCDW and UCDW, where fluxes in the ACC exceed 30 W m^{-2}.

Winter double diffusive heat fluxes, calculated as above, tend to extend deeper into the water column than they do in the fall by 10 to 20 m; however, the maximum heat flux remains at about 10 W m^{-2} (Figures 21a and b). Similar calculations, for transects sampled during the other cruises, indicate that spatial and temporal variability in the double diffusive heat flux is small and subtle differences which occur are within the accuracy of (14) and the data used (analysis not shown).

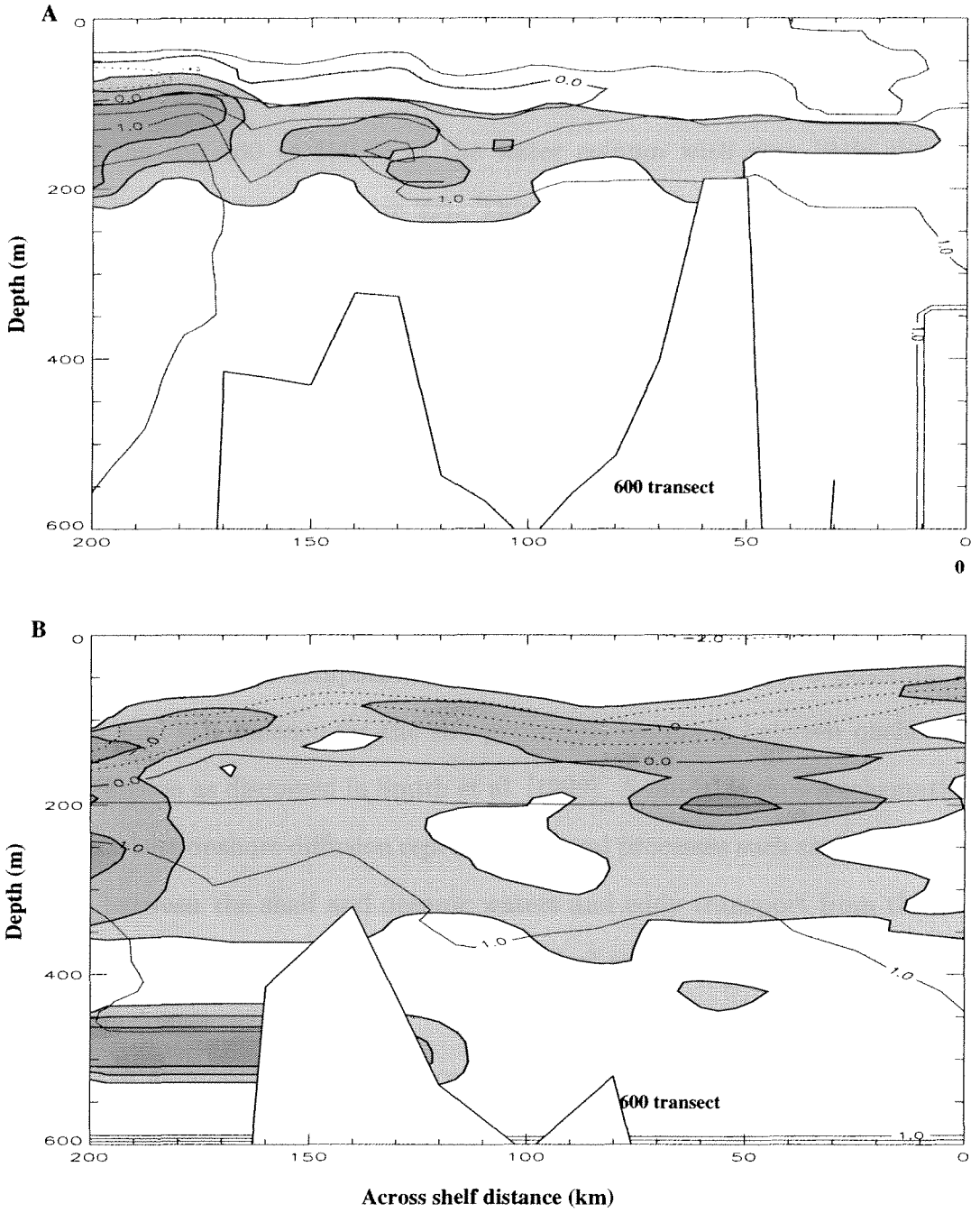

Figure 21. Fall and winter double diffusive heat fluxes for the 600 transect. Across shelf distribution of potential temperature (°C) for the 600 transect for the A) fall and B) winter 1993. The 5, 10 and 20 W m^{-2} double diffusive heat flux regimes are shaded as reference (lighter to darker for increasing fluxes). Temperature contours are for -2 to 1.5°C in 0.5°C intervals with dotted lines for negative values.

4.2 Bulk ocean budgets

The vertically averaged distributions of temperature and salinity indicate that most hydrographic variability between cruises during the 1993-94 sampling season occurred in the top 100 to 150 m of the water column with very little change in the sub-pycnocline waters (Figure 22). This result is consistent with the statistics calculated on the σ=27.74 (Figure 3) and confirms an analysis of historical data [Hofmann et al., 1996] indicating that the sub-pycnocline shelf waters to the west of the Antarctic Peninsula exhibit little variability over longer time scales. A station-by-station comparison of the temperature and salinity distributions [Klinck, 1998] indicates that subtle changes in the sub-pycnocline hydrography occurs and may be related to variability in the location of ACC relative to the west Antarctic Peninsula shelf break.

Given the persistent temperature and salinity characteristics, a potential first order heat and salt balance for the sub-pycnocline waters is between onshore and vertical diffusion as discussed in Smith et al. [1999]. A model is shown schematically (Figure 2) where onshore diffusion represents several processes such as diffusion down gradients between the shelf and oceanic waters and eddy transport from the ACC. Likewise, the processes represented in the vertical are down-gradient diffusion and double diffusion.

With the assumptions of a balance between onshore and vertical diffusion, (1) yields

$$\begin{aligned} HK_h^T \frac{\partial T}{\partial x} - LK_v^T \frac{\partial T}{\partial z} &= 0 \\ K_h^S H \frac{\partial S}{\partial x} - LK_v^S \frac{\partial S}{\partial z} &= 0 \end{aligned} \tag{40}$$

which is a set of two equations with four unknowns, K_h^T, K_h^S, K_v^T and K_v^S.

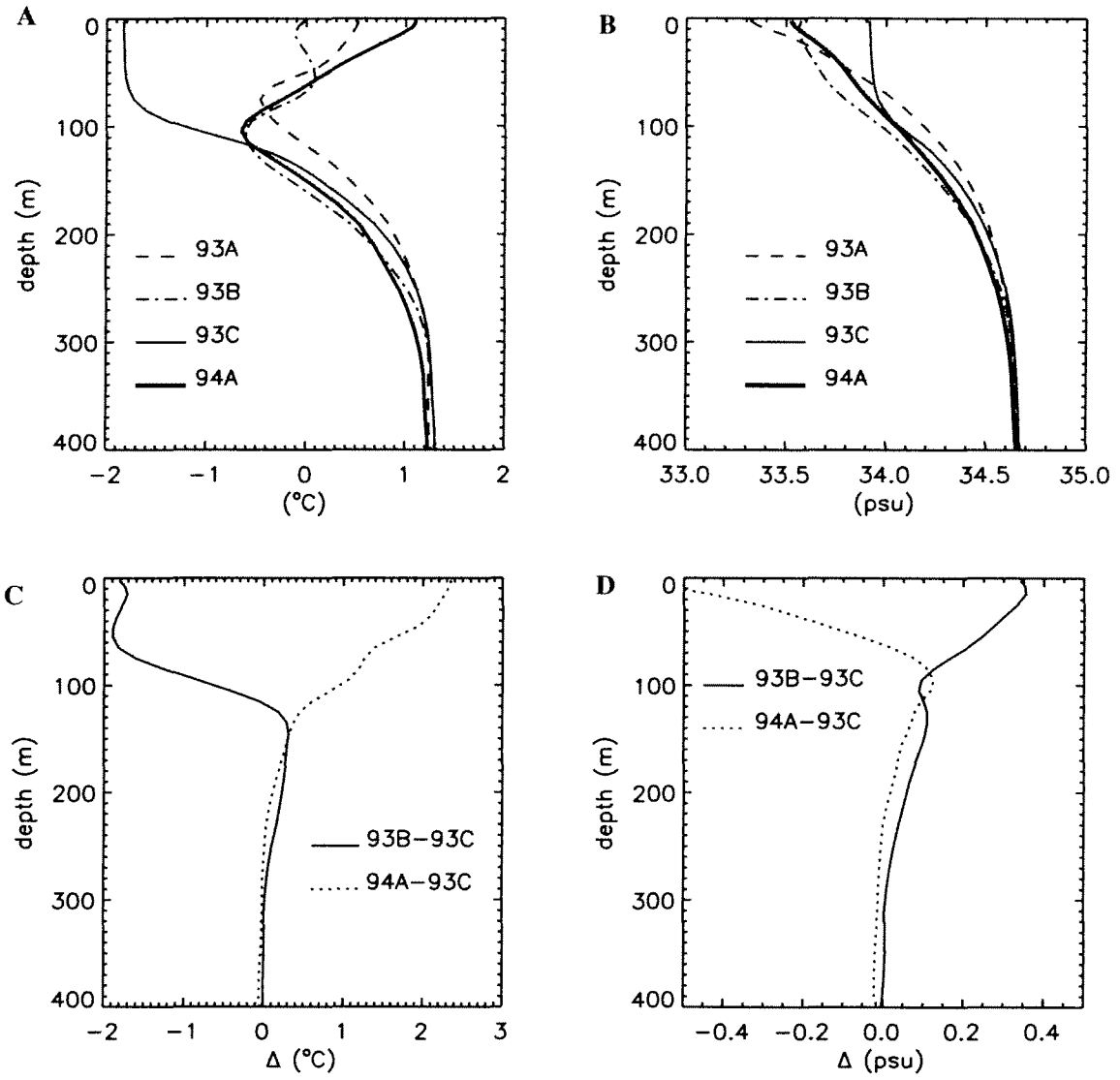

Figure 22. Shelf hydrography and hydrographic changes between cruises during the 1993-94 sampling season. Vertical distributions of the A) average temperature, B) average salinity, C) fall to winter and winter to summer temperature change and D) fall to winter and winter to summer salinity change calculated using observations from the west Antarctic Peninsula shelf.

The equations can be further reduced by assuming that horizontal diffusion is the same for heat and salt (i.e. K_h^T=K_h^S). Based on the results given in Section (4.1.3) the analogous assumption cannot be made in the vertical (i.e. $K_v^T \neq K_v^S$) thus allowing for differential, vertical transfer of heat and salt.

Given reasonable choices for horizontal diffusion of $K_h^T = K_h^S = 10$ to 100 m^2 s^{-1} [Klinck, 1998; Smith et al., 1999] the balancing vertical fluxes are found with $K_v^T = 1{\times}10^{-5}$ to $1{\times}10^{-4}$ m^{-2} s^{-1} and $K_v^S = 8{\times}10^{-7}$ to $8{\times}10^{-6}$ m^{-2} s^{-1}. The horizontal salinity gradient would need to be nearly an order of magnitude greater than observed to maintain a balance with $K_v^T = K_v^S$. This result is consistent (within an order of magnitude) with the results from the MC76 double diffusive calculation presented in the previous section (Section 4.1.3) and indicates that the observed sub-pycnocline hydrography can be maintained under the balance of horizontal and vertical diffusion. The most consistent balance is achieved with different vertical diffusion coefficients for heat and salt. double diffusion has an important role in the vertical transfer of heat and salt across the permanent pycnocline along the western Antarctic Peninsula.

Seasonal changes in the thermohaline properties of AASW occur (Figure 22) and the average heat and salt fluxes necessary to produce the observed changes can be found by

$$\begin{aligned} Q_H^{av} &= \int_{z=h_l}^{z=h_u} \rho_o C_p \frac{\partial T}{\partial t} \cdot dz \\ Q_S^{av} &= \int_{z=h_l}^{z=h_u} \rho_o \frac{\partial S}{\partial t} \cdot dz \end{aligned} \tag{41}$$

where $\frac{\partial T}{\partial t}$ and $\frac{\partial S}{\partial t}$ are approximated by the temperature and salinity changes between cruises and the thickness of the AASW layer (0 to 110 m) defines the upper ($z = h_u$) and lower ($z = h_l$) limits for the integrals.

The observed AASW hydrographic changes from the fall (93B) to the winter (93C), correspond to an average heat flux loss of 47 W m^{-2} and a salinity fluxes of 1.5 mg salt m^2 s^{-1}. Conversely, the heat gain and flux of salt from winter to the summer (94A) are 40 W m^{-2} and -1.0 mg salt m^{-2} s^{-1}.

The time-integrated heat budget for the ice-free heat flux (Figure 23) shows an annual cycle in heating and cooling. Similar calculations which include the contributions from double diffusion and ice processes are also presented (Figure 23) as an indication of overall closure for the heat budget.

The average cooling for AASW between the 93B and 93C cruises is 73 W m^{-2} which is found by calculating the average slope of the solid curve in Figure 23 between days 110 and 225. The cooling is reduced to be 70 W m^{-2} (using the dashed curve in Figure 23) and 72 W m^{-2} (using the dotted curve in Figure 23) when accounting for heating from double diffusion and heat losses to ice, respectively. The average heating during the transition from winter to summer (93C to 94A) is 30 W m^{-2} and increases to 32 and 35 W m^{-2} when accounting for double diffusion and heat losses to ice, respectively.

The change in the salt content of the upper 100 to 150 m of the water column can be estimated for the same times as a consistency check on the local budgets (Figure 22b and d). Neglecting sources of salt from sub-pycnocline waters, the salt fluxes are consistent with ice growth/melt rates of approximately 0.25 to 0.5 cm day^{-1}. These rates are reasonable for the west Antarctic Peninsula continental shelf waters and would result in 0.25 to 0.5 m of ice in 2 to 3 months. The persistent, vertical flux of salt through the permanent pycnocline (salt source for AASW) could be balanced by precipitation rates on the order of 0.3 m yr^{-1} which are well within the precipitation rates recorded along the west Antarctic Peninsula (Section 3.4.5).

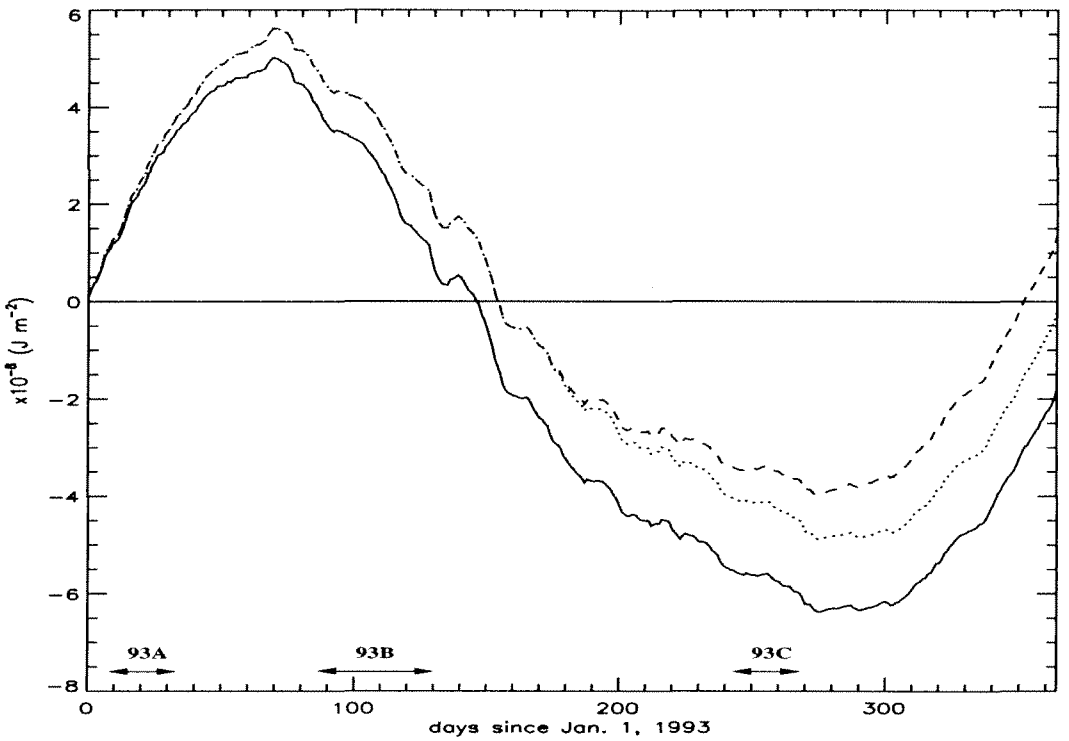

Figure 23. Time integrated 1993 heat budget ($\int Q_{open} \cdot dt$). The solid line represents the integration for the ice free, surface budget only while the dashed line represents the calculation with an assumed double diffusive heat flux of 5 W m^{-2} into AASW from below the permanent pycnocline. The dotted line is the same as the dashed with an assumed 10 W m^{-2} heat loss included in the calculation during times when the west Antarctic Peninsula shelf is ice covered. The times of cruises are indicated with arrows and the solid, horizontal line provides the zero reference for the calculation.

4.3 Results from a thermodynamic ice-mixed layer model

4.3.1 Model initialization, forcing and spin-up

A coupled, dynamic-thermodynamic, ice-mixed layer model (Sections 3.3 and 3.4) is initialized with observed temperature and salinity from August 1993 (Figure 12a) and an idealized area-averaged ice thickness of $A_i h_i$=0.5 m. The 1993 atmospheric time series from Faraday were repeated and used to force the model for an 8 year simulation so model spin-up and stability could be evaluated.

The simulated temperature and salinity of the mixed layer reproduced several key features of the ice-ocean system along the west Antarctic Peninsula including the timing of the ice cycle (i.e. timing of ice advance/melt and maximum extent), (Figure 24a-c) mixed layer depths (*mld*) and the depth of the permanent pycnocline. As in Kantha and Clayson [1994], the simulated *mld* is determined by the deepest point where the gradient Richardson number (Ri_g) exceeds the arbitrary threshold of 0.7 while the depth of the permanent pycnocline is determined by the depth 33.9 isohaline.

The simulated distribution of ice concentration adjusts from its initial winter conditions ($A_i h_i$=0.5 m to 0.3 m) by the second winter (i.e. -0.2 m yr^{-1}). During the second through fourth winters, the simulated ice field increases its winter maximum ice thickness by approximately 0.02 m per year. After year 3, the simulation stabilizes with a maximum winter concentration of .35 m, gaining less than 1 cm yr^{-1} of area averaged ice cover during the last 4 years of the simulation.

The top 150 m of model undergoes a slow drift towards fresher conditions as seen in the salinity field (Figure 24c) with isohalines deepening over time. This drift can be seen in all isohalines; however, it is most evident in the 34.0 contour since this salinity is generally deep enough to be removed from seasonal processes associated with ice and surface forcing. A similar drift can be seen in the temperature field as the model spins-up with the top portion of the model tending towards colder

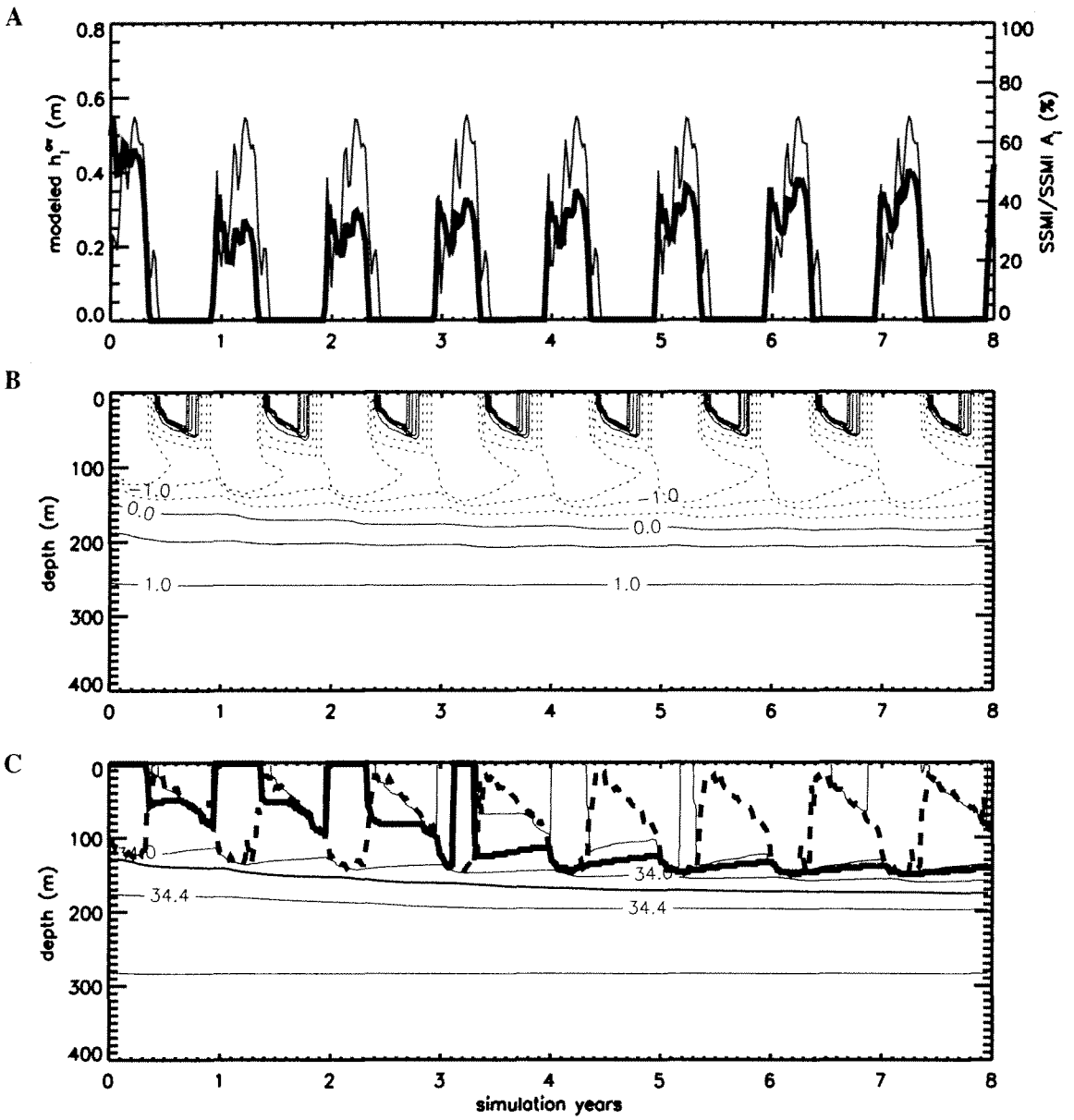

Figure 24. Simulated area averaged ice thickness and key hydrographic features for an 8 year model spin up. A) Area averaged ice thickness (thick line) and GSFC SMMR/SSMI near-Palmer ice record (thin line). B) Time and depth development of simulated temperature. Contours are for -2 to 2°C with a 0.5°C interval (negative contours are dotted). C) Time and depth development of simulated salinity. Contours are for 33.6 to 34.6 with a contour interval of .2. The position 33.9 isohaline is indicated with a thick line serves as a proxy for the depth of the permanent pycnocline. Mixed layer depths are illustrated by the thick dashed line.

conditions. This drift is most pronounced during the first four years of the simulation and most likely represents the period of time when the model adjusts its initial conditions to the prescribed forcing. Over the first four years, key features in the AASW (i.e. isotherms and isopleths) deepen at a rate of approximately 4 to 5 m yr^{-1}. After the fourth year, the model settles on a rate which is less than 1 m yr^{-1} and is considered to be stable. Some of this drift may be due to the oversimplification of precipitation (Section 3.4.5) or the missing physics associated with horizontal processes. As with the ice, the model appears to adjust after the fourth year when the simulated *mld* and the depth of the permanent pycnocline stabilize as suggested by a continuing deepening less than 1 m yr^{-1}. An annual cycle of the simulated *mld* and the depth of the permanent pycnocline develops and is discussed in the next section.

4.3.2 One year (1993) simulation

A one year record starting in the middle of model year 5 (01 January) is analyzed as the 1993 model simulation. The lack of recorded ice thickness along the west Antarctic Peninsula makes a direct comparison to observations difficult; however, the timing of growth and melt obtained from the simulations can be compared to the ice cycle observed in the near-Palmer GSFC SMMR/SSMI ice record (Figure 26). Simulated thermohaline distributions are compared to observed distributions as a further test of the model stability.

Ice cycle: Ice occurs in the model for 165 days (5.5 months) of the 365 day simulation (Figure 25a). Both observed and simulated ice fields, exhibit rapid growth beginning around day 150 (early May). The initial growth period lasts for several weeks and is followed by a period of alternating advance and retreat in ice cover. Around day 290 (mid-August), a rapid spring melt begins which persists until day 310 when the simulated ice cover vanishes. The transition from ice-covered to ice-

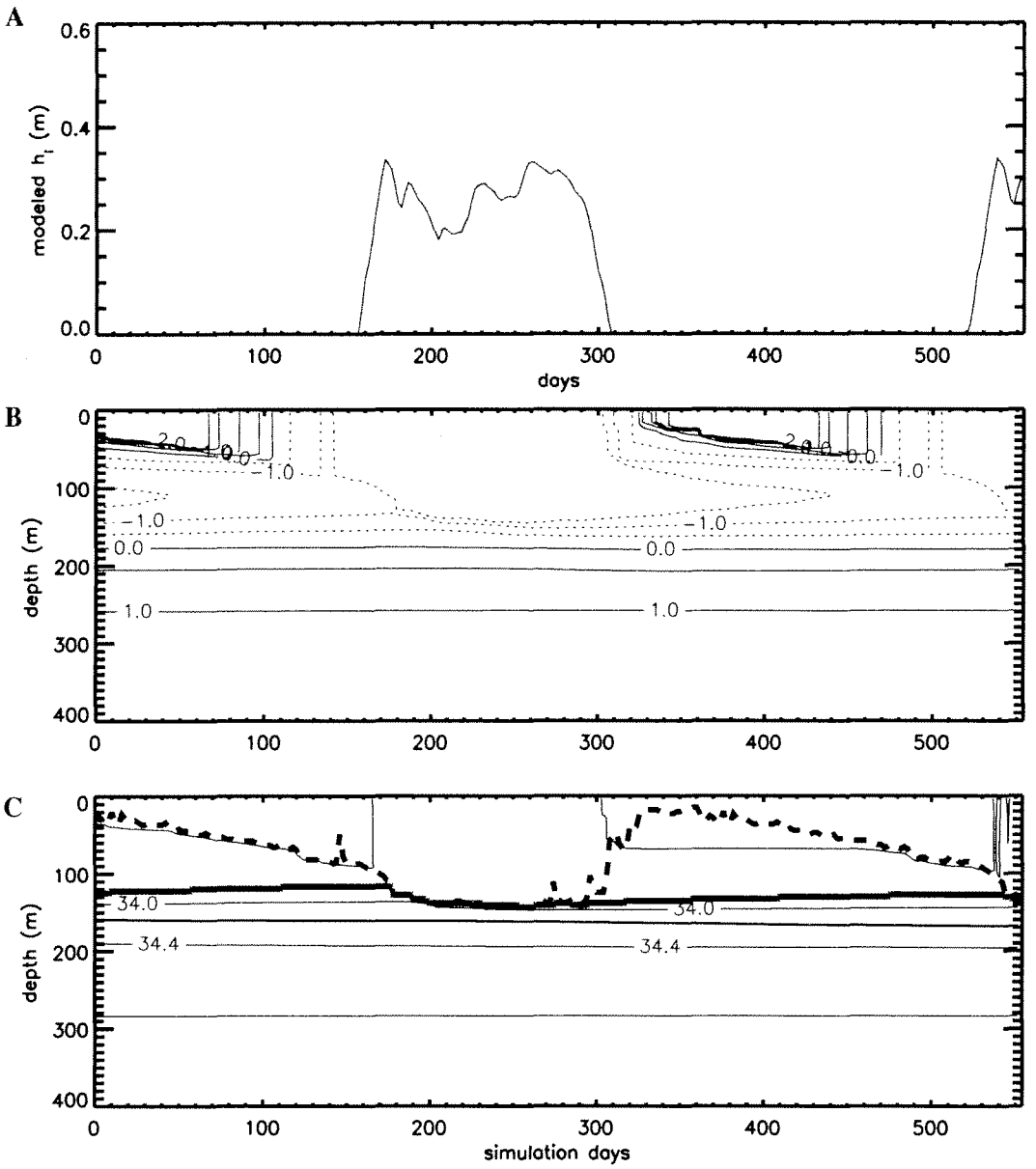

Figure 25. Simulated area averaged ice thickness and key hydrographic features for 1993. A) Simulated time distributions of area averaged ice thickness, B) depth and time distributions of temperature and C) salinity. Contour of model temperature with time. Temperature contours range from -2 to 2°C with a 0.5°C interval (negative contours are dotted) and salinity ranges are from 33.6 to 34.6 with a contour interval of 0.2. The position 33.9 isohaline is indicated by the thick, solid line and indicates the depth of the permanent pycnocline while mixed layer depths are indicated by the thick dashed line.

free conditions occurs faster in the simulated fields than in the observations (Figure 26a). Also, the model fails to reproduce the small observed peak between day 320 and 340. However, it is difficult to determine if the observed peak in ice cover at days 320 to 340 results from ice growth (thermodynamics) or from horizontal ice motion. Day 320 through 340 corresponds to a time of winds from the north which would tend to advect ice onshore. Horizontal advection is not allowed to contribute to changes in ice thickness in (23) and such an event would not be represented in the model. In addition to the overall timing of ice cycle, the ice simulations reproduce changes in ice thickness which occur on short time scales (a few days) (Figure 26a).

Heat fluxes and ice growth rates: During the rapid, initial ice growth (day 150 to 170 in Figure 26a), growth rates at the ice-ocean and the atmosphere-ocean interfaces are both positive (growth) and combine to produce a total growth rate on the order of 5×10^{-7} m s^{-1} (4 cm d^{-1}) (Figure 26b). This initial, rapid growth ends around day 170 when the growth at the base of the ice becomes negative and open ocean growth is reduced to nearly zero. From day 170 to the end of the ice cycle, melting at the ice-mixed layer interface is small with rates on the order of 0.3×10^{-7} m s^{-1} (0.5 cm d^{-1}) but persistent.

Throughout the 1993 simulation, the principal balance in (23) is between melting at the ice-ocean interface and growth at the atmosphere-ocean interface. The contribution from surface melting is significant only for a short time during the spring melt (e.g., notice that growth rates at the ice-ocean and atmosphere-ocean interfaces account for a large percentage of the total growth in Figure 26b). Periods of mid-winter ice retreat result when open ocean growth is either zero, or insufficient to counter the persistent melting at the ice-ocean interface. Conversely, ice growth is episodic and driven by ice formation in open water when oceanic ice formation is large compared to under ice melt. Many ice growth periods are characterized by

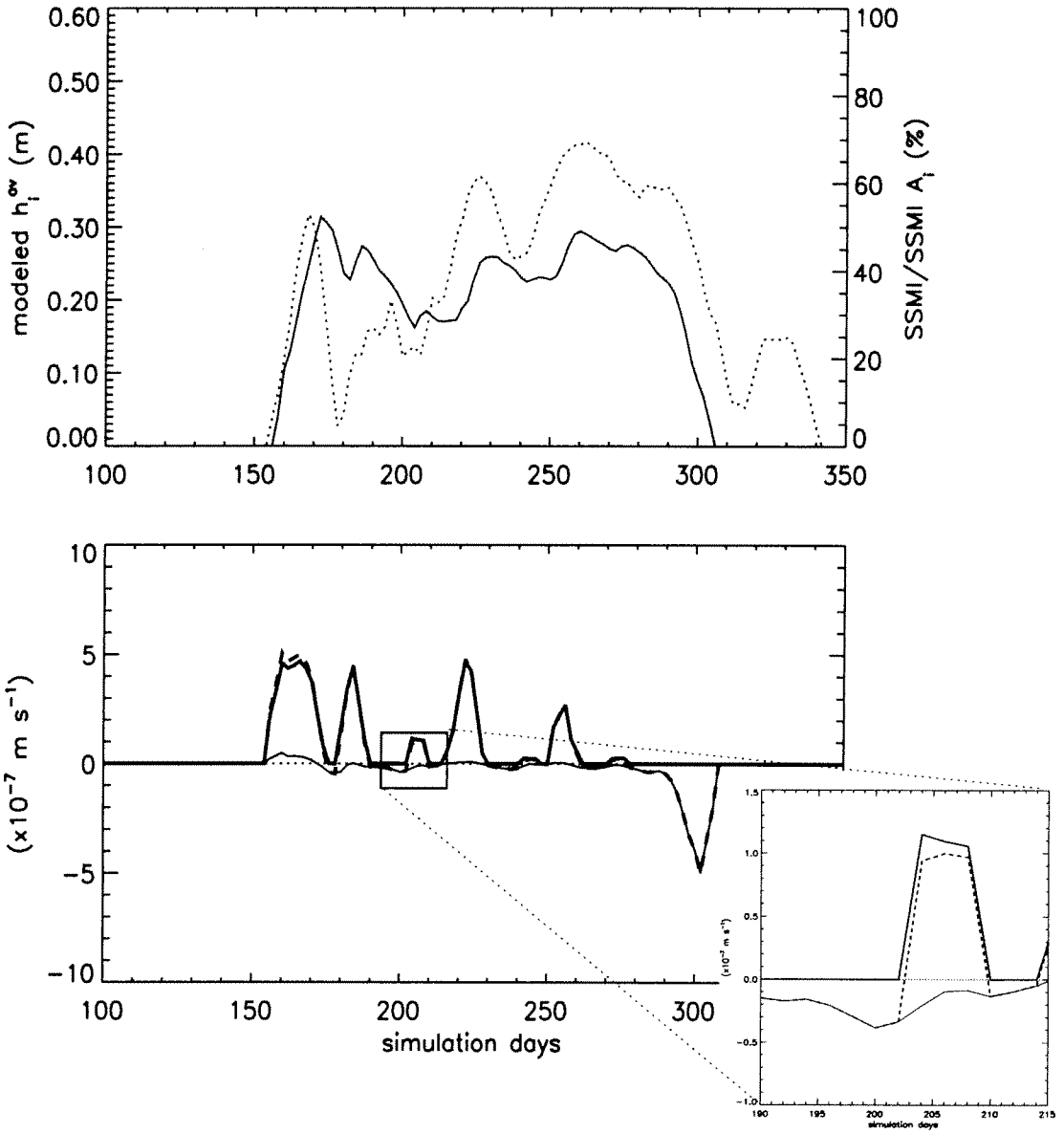

Figure 26. Simulated ice thickness, growth rates and the near-Palmer GSFC SMMR/ SSMI time series for winter 1993. A) Simulated (solid) and observed (dashed) sea ice for winter 1993. B) Simulated growth rates ($\times 10^{-7}$) for the simulation in A) with Wao (thick), Wio (thin) and total growth rate (W) (dashed) indicated. Zero growth is indicated with the horizontal dotted line and an expanded view of days 190-215 is provided in the insert.

open ocean growth rates in excess of 4×10^{-7} m s^{-1} (5 cm day^{-1}). An example of the competition between open ocean ice growth and melting under the ice is illustrated between days 185 and 200, at which time formation of ice in the open ocean is essentially 0 m s^{-1}, while melt rates at the base of the ice are on the order of 0.02 to 0.05 m s^{-1}. During this time, the area-averaged ice thickness is reduced by nearly 0.08 m. Open ocean growth rates becomes non-zero (around day 200), corresponding to cold atmospheric temperatures and large open ocean, sensible heat losses (see day 200 in Figures 16b, 18b,c and 26a,b), at which time ice grows.

The spring melt begins around day 290 (September-October) and is dominated by intense under-ice melting that occurs at a rate of 5×10^{-7} m s^{-1}, which is sufficient to reduce the ice cover from its maximum winter value to ice free conditions within 20 days.

The model open ocean heat budget is similar to the budget calculated in Section 4.1.2 (Figures 18c and 27a). In addition to heat fluxes calculated for ice-free conditions (Section 4.1.2) exchanges of heat between the AASW and the ice are included in the model (Figure 27b). Excluding the peak in heat flux between the AASW and the ice (Qio) around day 300, the average winter heat loss from AASW to the sea ice is 10 W m^{-2} (cooling surface waters). The peak ice-free heat flux is on the order of 100 W m^{-2} occurs during the spring melt, and is driven by solar warming. The elevated heat fluxes are initiated, and dominated, by heat input into the ice-free leads. Increased SST then drives the large, negative under ice melt and spring melt. As in the calculation of the ice-free heat budget (Section 4.1.2) the total, modeled heat flux (Figure 18a) becomes positive in the spring as a result of increased solar heating.

Salt fluxes associated with brine rejection and melting (Figure 27c) occur only with ice cover. Integrating the salt flux over the annual cycle results in a net input of fresh water which is equal to the prescribed precipitation (i.e., approximately

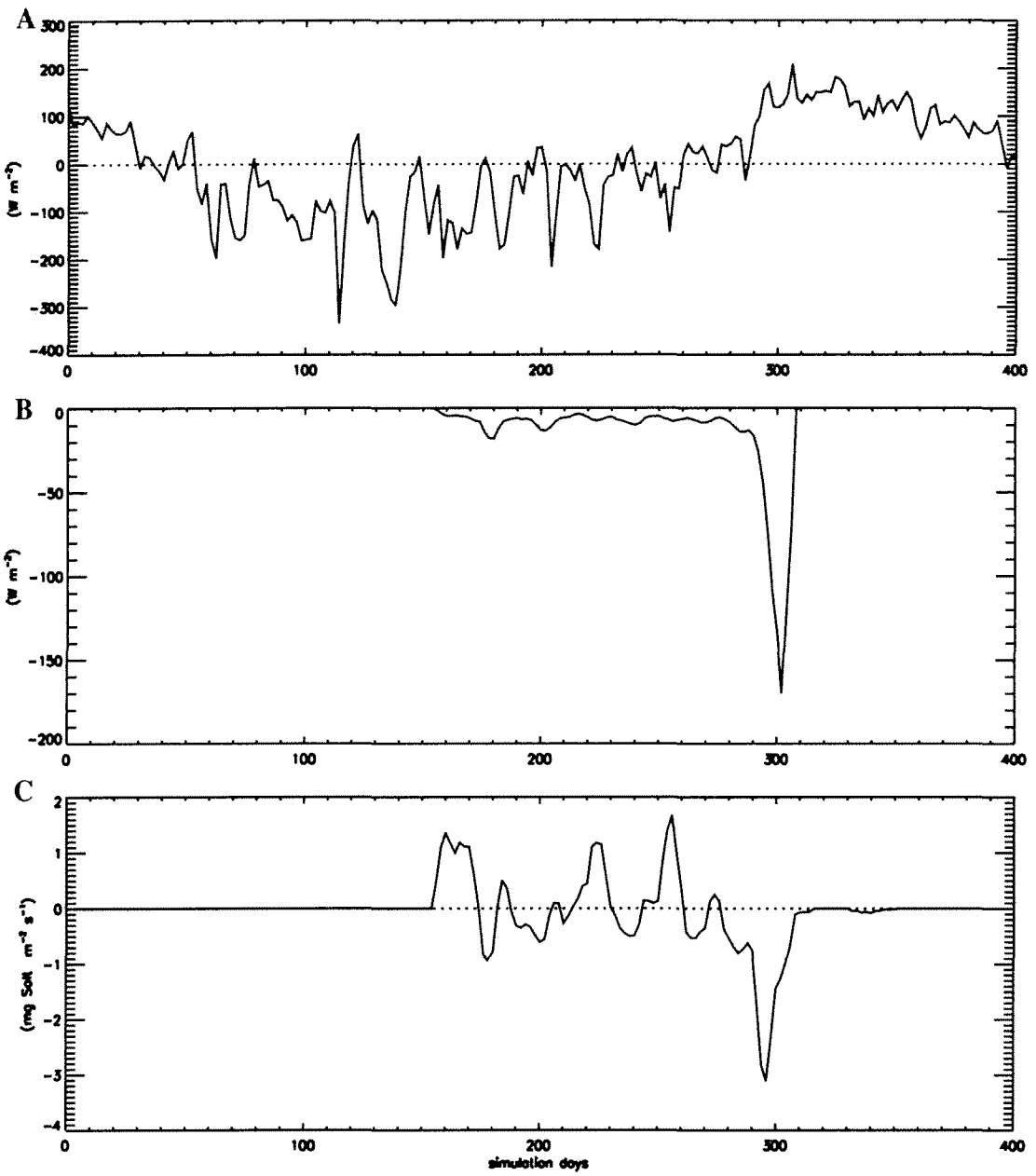

Figure 27. Heat and salt budgets from the 1993 simulation. A.) Simulated ice free heat budget calculated from the model using 1993 atmospheric data from Faraday station. B.) Simulated heat flux at the ice-ocean (Qio) interface (negative indicating heat loss from AASW). C.) Simulated salt flux associated with ice processes. Zero salt flux is indicated by the horizontal dotted line.

0.5 m). This comparison provides a consistency check and indicates that horizontal advective processes are not dominant and that the salt fluxes associated with the ice cycle are closed (i.e. freshening during ice melt cancels brine rejection during ice growth). The fresh water input via precipitation is needed to balance the persistent flux of salt from modified-UCDW to AASW.

Hydrographic cycle: Winter AASW hydrography is characterized by T=-1.9°C and S=33.8 extending from the surface to a depth of approximately 140 m (Figure 25b,c). These well mixed conditions persist throughout the winter period (day 200 to 300) of the simulation when ice cover is present. The surface layers warm, and freshen, around day 300 as surface heating drives the spring ice melt, which results in significant surface stratification (Figure 25b,c) and shallowing of the mixed layer (Figure 25c and 28a). The surface waters continue to warm (mainly) and freshen (slightly) throughout the summer due to solar heating and precipitation. The persistent erosion of the spring stratification can be seen as the *mld* deepens throughout the year due to surface wind mixing (Figure 25b,c). The simulated summer *mld* is typically between 40 and 80 m (Figures 25c and 28a,b) and peak surface temperatures and minimum salinities are 3°C and 33.65, respectively. These conditions are about 0.5 to 1°C warmer and 0.5 saltier than observed with the differences most likely due to insufficient surface mixing or the lack of horizontal processes in the model.

During the fall, surface temperatures decline under the influence of surface cooling (days 400 - 500, Figure 25b) which drives deeper mixing and accelerated erosion of the *mld*. Simulated surface salinities increase slightly during this time as deeper mixing injects salt into the upper water column. The salinity for AASW returns to winter values as sea ice forms and brine is injected into the surface waters. The simulated fall *mld* is around 80 to 100 m deepen to 120 m in the winter. Around

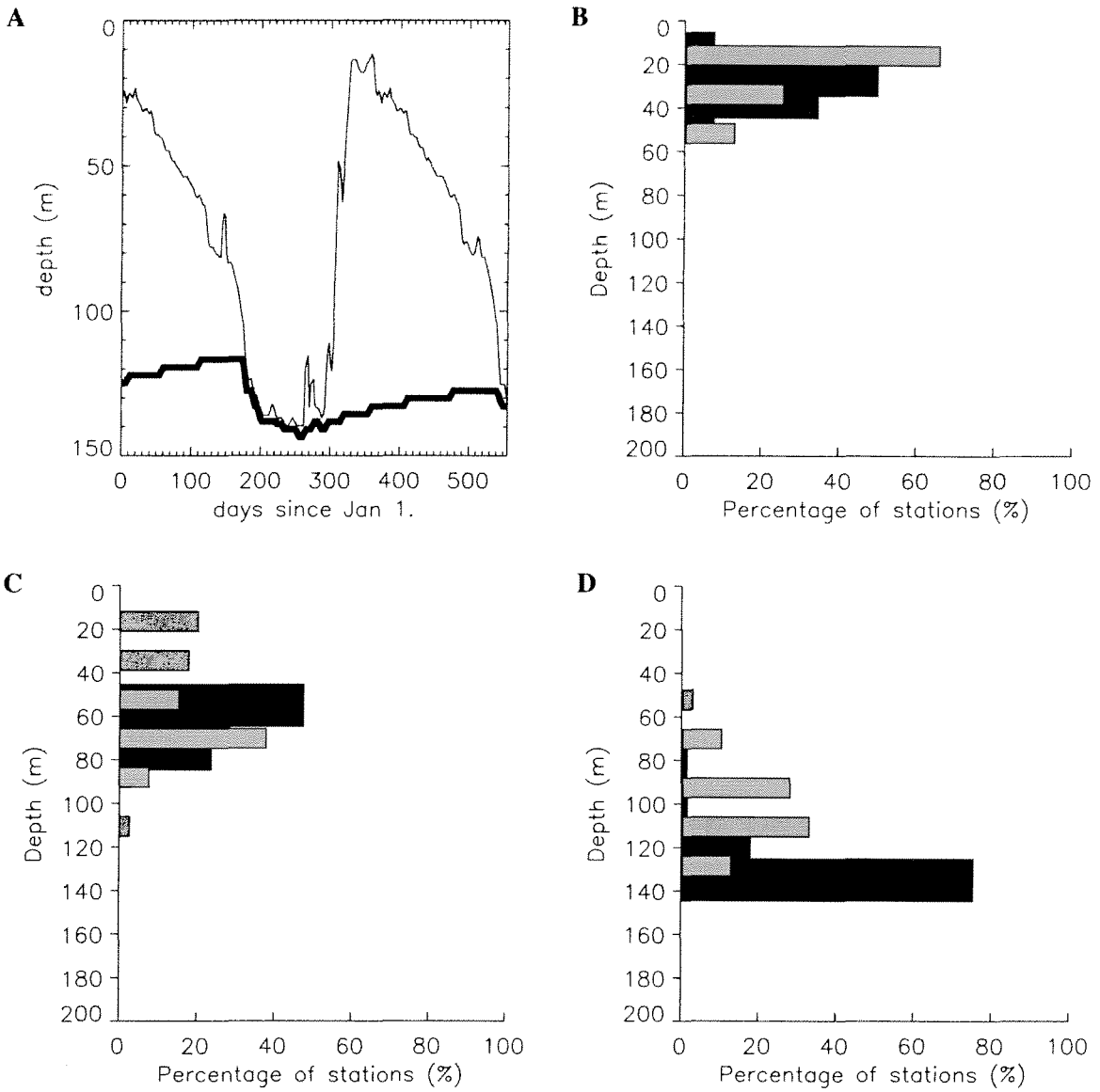

Figure 28. Simulated mixed layer and permanent pycnocline depths and hydrographic statistics. A) Simulated mixed layer (thin) and permanent pycnocline (thick) depths. Frequency distribution of simulated mixed layer depth for B) summer ($0 < \text{day} < 60$), C) fall ($90 < \text{day} < 130$) and D) winter ($180 < \text{day} < 220$). Times were chosen to coincide with the west Antarctic Peninsula cruises (Table 1).

day 150, the *mld* intersects the permanent pycnocline indicating that AASW is well mixed.

The permanent pycnocline is deepest (140 m) during the winter. When stratification exists within AASW (i.e. the formation of a seasonal pycnocline) the permanent pycnocline shallows somewhat as WW warms and becomes more salty from the input of heat and salt from below. This shallowing continues until stratification is eliminated within the AASW in winter and the permanent pycnocline depth is returns to its winter position. The overall trend in the simulated *mld* agrees with those from observations (Figure 28b-c); however, the model tends to mix excessively with *mld's* extending deeper than in the observations. This most likely is due to an over estimate of under ice stresses due to large ice velocities; a common result in models which use the free drift ice momentum equations [Steel et al., 1989].

Mixing regimes: The 1993 simulated ice field and two of individual components of the vertical mixing scheme (Sections 3.3.2 and 3.3.4) are presented in Figure 29. The MY2.5 turbulence closure scheme determines the mixing depth due to competing factors of wind induced mixing and buoyancy forcing. The deepest mixing occurs in the winter when freezing causes brine rejection and surface stress includes mixing at the open water interface and from under ice sources. Simulated winter mixing reaches depths of 120 to 140 m corresponding to mixing coefficients on the order of 0.1 to 0.01 $m^2\ s^{-1}$. The shallowest penetration of turbulent mixing occurs during the spring as a result of surface stratification due to fresh water input from melting ice and from surface heating. Simulated spring mixing coefficients are typically 0.01 to 0.001 $m^2\ s^{-1}$.

Mixing associated with double diffusion (K^T_{dd}= 5×10^{-5} to 10^{-4} $m^2\ s^{-1}$ and K^S_{dd}=5×10^{-6} to 10^{-5} $m^2\ s^{-1}$, respectively) occurs throughout the simulation; the maximum double diffusive heat flux is about 10 W m^{-2} (Figure 30a). Consistent

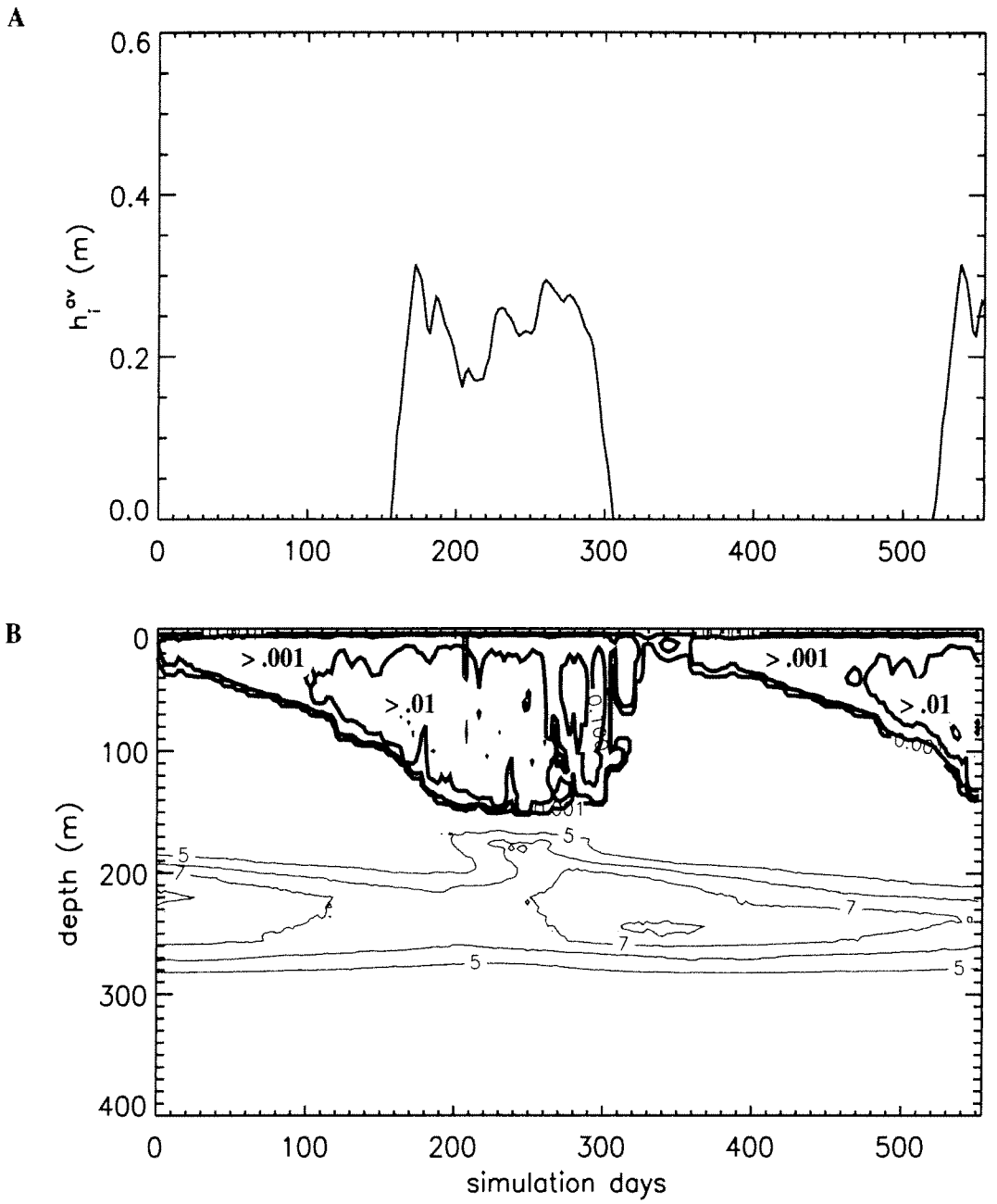

Figure 29. Mixing regimes during the 1993 simulation. A) Simulated, area-averaged ice thickness. B) Simulated vertical mixing coefficients for heat. Mixing coefficient associated with the MY2.5 scheme are indicated with thick contours while the coefficient associated with double diffusion are indicated with the thin contours. Contour levels for the MY2.5 mixing coefficient are 0.001, 0.01 and 0.1 while contour levels for double diffusion are 3×10^5 to 10×10^5 with a contour interval of 1×10^{-5}.

with the hydrographic data (Section 4.1.3), the maximum effects of double diffusion occur in the mid-pycnocline. where vertical gradients in temperature and salinity are maximum (Figure 29b). Gradient Richardson mixing contributes only for a few time steps during spring when surface stratification significantly reduces the ability of turbulence closure to break down the surface stratification. Otherwise, the vertical mixing coefficient from the MY2.5 turbulence scheme ($K_v^{MY2.5}$) is several orders of magnitude larger than any other mixing processes in the model, and thus, dominates mixing in the water column.

Nudging: The contribution of the nudging terms in (18) and (19) to the simulated distributions is found by vertically integrating (22) (using $\rho_o C_p$T for heat and ρ_oS for salt) from the surface of the model to the bottom. The resulting fluxes are the sources of heat and salt necessary to maintain the hydrographic character of the modified-UCDW (Figure 30a) and serve as an internal consistency check for how well the model is performing.

Results from this integration (Figure 30a) indicate that typical values for the replacement fluxes of heat (Q^T_{nudge}) and salt (Q^S_{nudge}) are 8 to 12 W m^{-2} and 0.5 to 0.6 mg salt m^{-2} s^{-1}, respectively and are fairly persistent throughout the simulation.

The integrated heat and salt fluxes in Figure 30a can be converted to effective mixing coefficients and compared to the results of the box model calculation presented in Klinck [1998] and in Smith et al.[1998]. These fluxes are converted using

$$K_h^T = \left(HQ^T_{nudge}\right)\left(\rho_o C_p \frac{\partial T}{\partial x}\right)^{-1}$$

$$K_h^S = \left(HQ^S_{nudge}\right)\left(\rho_o \frac{\partial S}{\partial x}\right)^{-1} \qquad (42)$$

where shelf dimensions and hydrographic values are summarized in Figure 2. The

resulting mixing coefficients from (42) are approximately 15 m^2 s^{-1} for heat and salt (Figure 30b) which are similar the the values presented in Klinck [1998] and in Smith et al., [1999] and balance vertical heat losses associated with the vertical mixing terms in (18).

4.3.3 Sensitivity to sub-pycnocline heat fluxes

Given the potential source of heat and salt to AASW from the sub-pycnocline modified version of UCDW (Section 2.2.1), a series of numerical experiments were designed to test the sensitivity of the simulated distributions to the sub-pycnocline water is presented in this section. As in the reference 1993 simulation, each experiment was initialized with the hydrographic distributions illustrated in Figure 12a and spun up to a similar state of equilibrium. Results from the from these equilibrium (fifth year) of each simulation are compared to the fifth year results from the 1993, reference simulation.

The experiments are divided into two categories: sensitivity to changes in the temperature of the sub-pycnocline waters, and sensitivity to the parameterization of the double diffusive fluxes of heat and salt.

Temperature of the sub-pycnocline water: The initial conditions associated with the shelf sub-pycnocline waters (Figure 12a) were shifted by -0.75, -0.50, -0.25, 0.25, 0.50 and 0.75°C giving a total range in sub-pycnocline temperatures of 0.45 to 1.95°C. All other model processes and parameters are held constant. The lower end of the temperature range is colder than any shelf measurements in the historical data base [Hofmann et al., 1996] while the upper end corresponds to temperatures associated with UCDW found on the oceanic side of the shelf break Smith et al. [1999].

Increasing the temperature of the sub-pycnocline water reduces the overall thickness of the ice at the time of maximum winter ice extent (day 290) (Figure 31a)

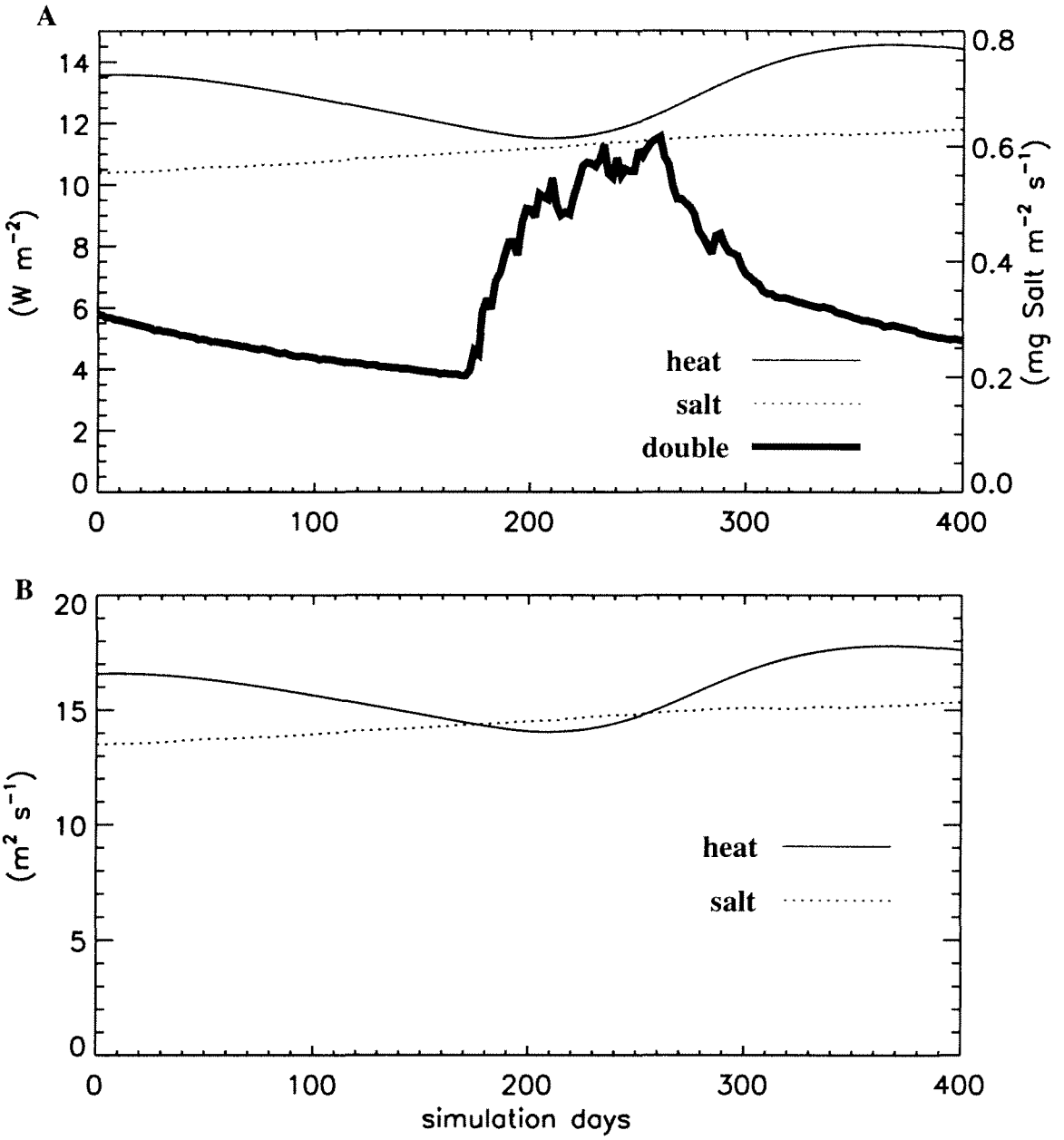

Figure 30. Oceanic fluxes of heat and salt through the permanent pycnocline during the 1993 simulation. A) Vertically-integrated heat and salt fluxes resulting from nudging (Equation 22) with the maximum double diffusive heat flux. B) Horizontal diffusion coefficients for heat and salt (Equation 1) calculated from the vertical fluxes of heat and salt in A).

while decreasing the temperature results in thicker ice. A temperature increase of 0.75°C reduces the average ice cover by half (Figure 31c) while decreasing the temperature by a factor of two results in 30% increase in simulated ice cover (Figure 31c).

The timing of the ice cycle is unaffected by changes in the sub-pycnocline temperature. In all simulations, rapid ice growth starts around day 150 and lasts for several weeks. Similarly, the spring ice retreat begins near day 290. Ice-free conditions occur earlier in the simulation with thinner ice (warmer sub-pycnocline water) but this is due to a smaller quantity of ice rather than an increased melt rate.

Simulated mixed layer and permanent pycnocline depths were only slightly affected by the changes in the sub-pycnocline temperature. Shallower *mld* resulted in simulations with thicker winter ice (cooler sub-pycnocline temperatures) while deeper *mld* were produced with reduced ice cover (warmer sub-pycnocline temperatures). The depth of the permanent pycnocline changes very little.

Parameterization of double diffusion: The mixing coefficients associated with double diffusion (K_{dd}^{T} and K_{dd}^{S}) were scaled by factors of 0.0, 0.5, 1.5. 2.0 and 3.0 while all other model processes and parameters held constant. Removing double diffusion ($K_{dd}^{T,S}$=0) resulted in a 50% increase in average winter ice thickness, while doubling double diffusion resulted in averaged winter ice thickness reduced by nearly 50% (Figure 31b,d). If double diffusion is increased by a factor of three, ice free conditions occur during mid-winter (day 224, Figure 31b).

As found for the simulations with modified sub-pycnocline water temperatures, the effect of changed vertical heat fluxes on simulated ice thickness at the time of maximum winter ice extent was less pronounced than for the average winter ice thickness (Figure 31d). The timing of the ice cycle was essentially unchanged with different double diffusive fluxes.

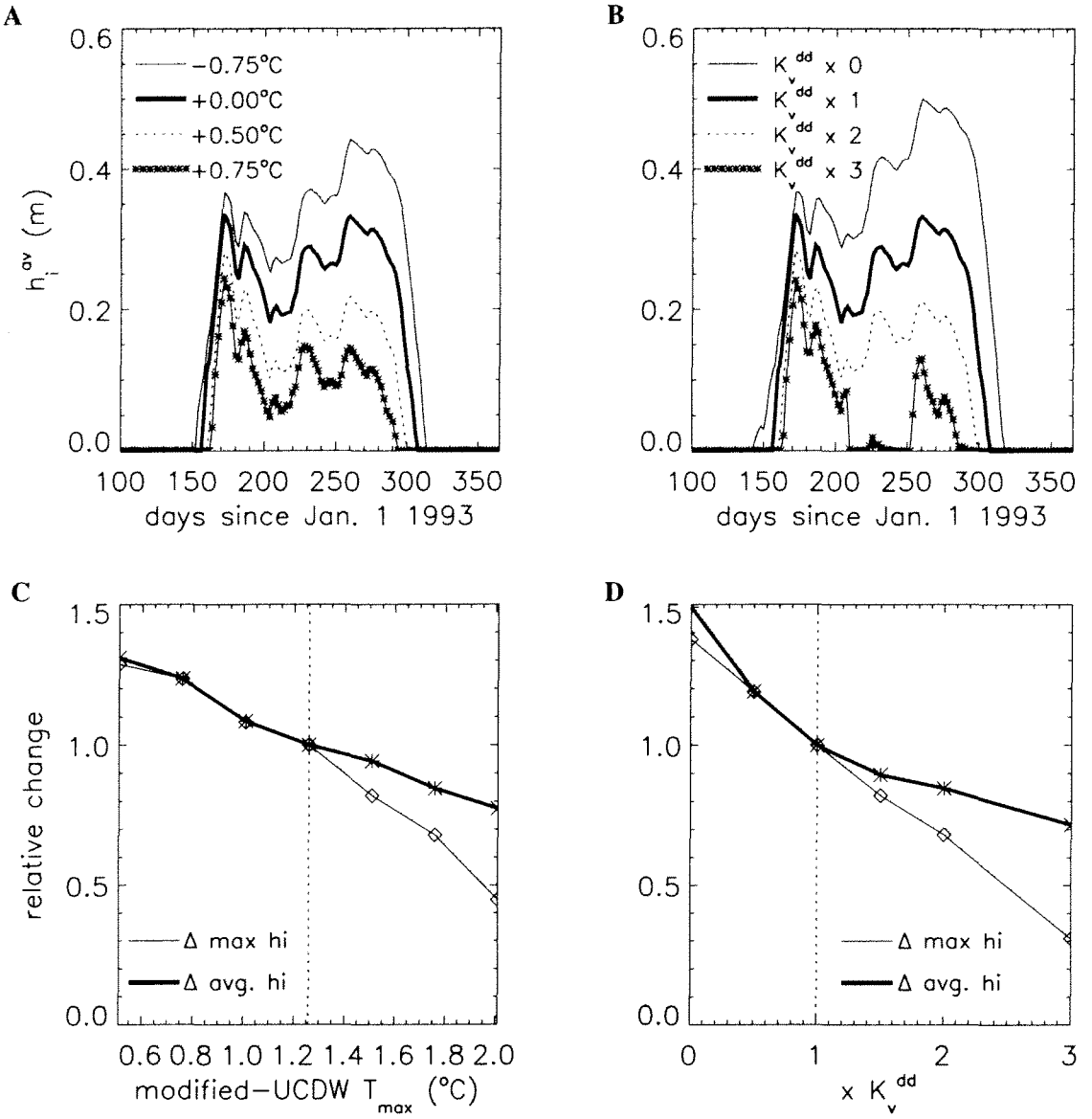

Figure 31. Area averaged ice thickness with changes in sub-pycnocline temperatures and double diffusive parameterization. A) Simulated area-averaged ice thickness for the reference case (temperature shifted by 0°C) and with shifts in the sub-pycnocline temperatures. B) Same as A) except for changes in the parameterization of double diffusion (K_v^{dd}) C) Changes in maximum winter ice thickness and average winter ice thickness for simulations presented in A) (the reference simulation is indicated with the vertical dotted line) D) Same as C) except for simulations presented in B).

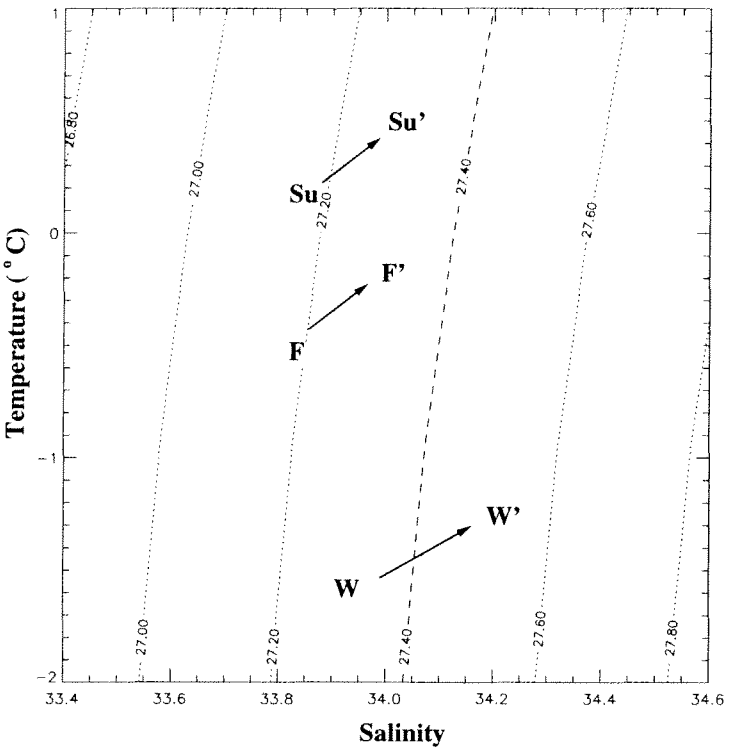

Figure 32. Surface water temperature and salinity averages for the base 1993 simulation with double diffusive effects turned off. Simulated, average winter (W), fall (F) and summer (S) temperature (°C) and salinity (psu) for AASW from the 1993 reference simulation (non-prime) and from a simulation using a constant background diffusive flux instead of the double diffusive mixing scheme (').

Changes in double diffusive heat fluxes and horizontal heat replacement from the nudging (Figures 29 and 30a) have similar effects. Increases in double diffusion produce slightly deeper spring *mld* due to reduced ice cover while reductions in double diffusion results shallower *mld* due to increased ice cover. The depth of the permanent pycnocline is slightly shallower for simulations with increased K_{dd}.

An additional simulation done in which the double diffusive effects were replaced by a constant background diffusion of (α_{bkgrnd}=5×10^{-5} m^{-2} s^{-1}) for both temperature and salinity. This simulation represents the default mixing scheme used in the MY2.5 mixing scheme. The simulation produces reasonable temperatures for AASW (Figure 32), but salinities are generally too high. In particular, winter AASW salinities are in excess of the maximum observed winter values of 34 [Hofmann and Klinck, 1998].

4.3.4 16 year (1978-1994) simulation

The sixteen year record (1978-1994) of atmospheric conditions at Faraday Station provide the opportunity to simulate ice conditions which can be compared to the GSFC SMMR/SMMI ice observations from the same time period. The reference 1993 simulation (discussed in the previous section) is used as initial conditions for the sixteen year simulation. The daily average meteorological conditions at Faraday Station force the 1978-1994 simulation.

The modeled ice cycle reproduced many of the high/low (as defined by departure from the sixteen year average [Smith et al., 1996]) ice years observed in the GSFC SMMR/SSMI ice field (Fig 33a,b). In particular, the model reproduced the record low and high ice years in 1989 and 1987 reported by Comiso et al. [1993] and others. As in the observed ice field, the model simulated high ice years in 1980, 1981 and 1982 and low ice years in 1983, 1984 and 1985. The high ice conditions in 1980 was not produced by the model and may result from imposing climatology in the

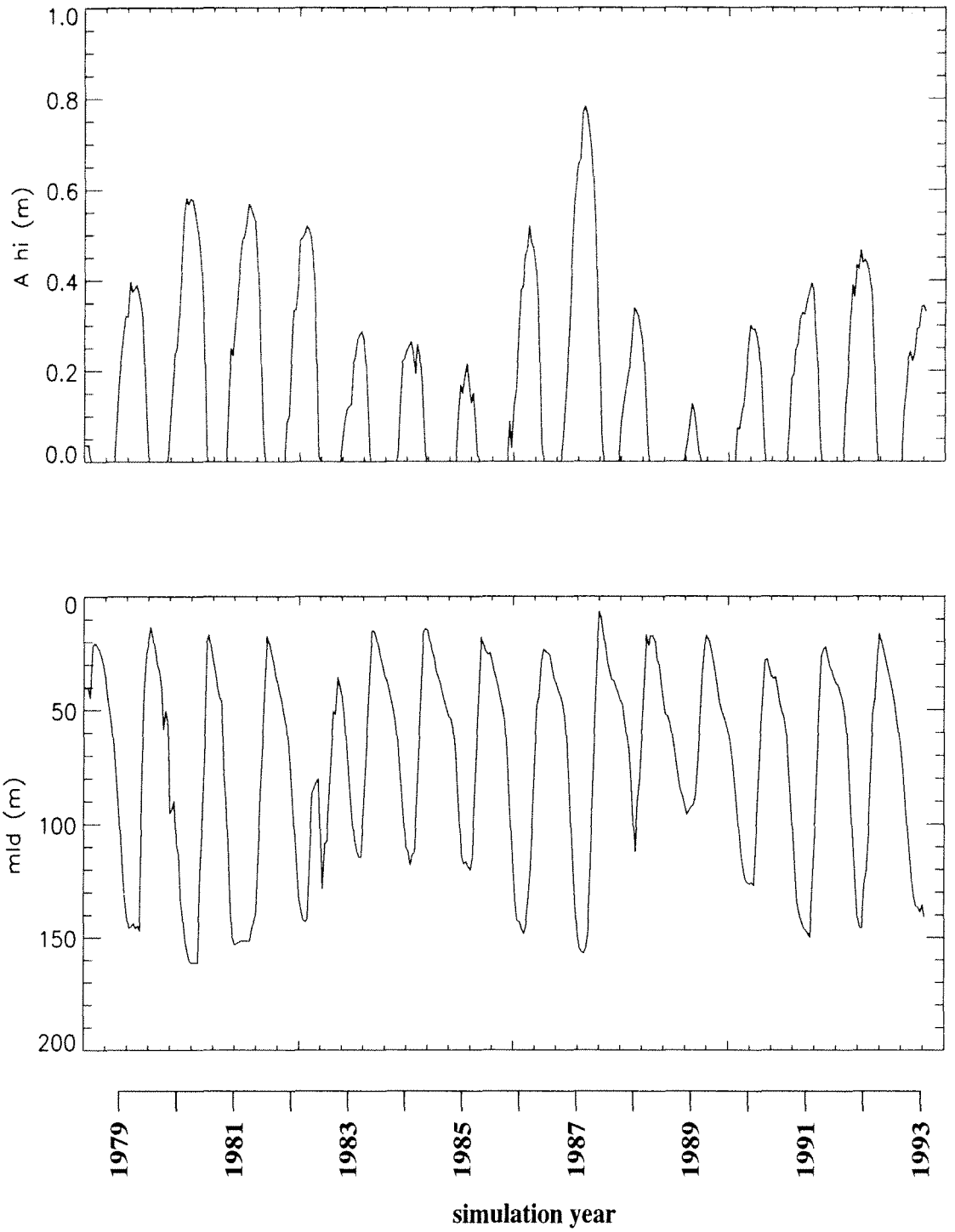

Figure 33. Results from a simulation forced with daily averaged atmospheric conditions from Faraday Station over a 16 (1978-1993) year period. A.) Simulated area-averaged ice thickness and B.) the depth of the mixed layer.

sub-pycnocline waters through nudging. Minimum spring *mld* were 10 to 30 m, with the deeper *mld* following years with low ice cover (Figure 33b). The depth of the permanent pycnocline was nearly 50 to 70 m shallower in low ice years (Figure 33b).

CHAPTER 5
DISCUSSION

The ice-free heat flux calculation (Section 4.1.2) provides a context for evaluating, ranking and quantifying important processes which affect the of sea-ice distribution and hydrographic structure of the west Antarctic Peninsula continental shelf. In addition, the numerical simulations provide a mechanism to investigate processes at the atmosphere/ice/ocean interface and to evaluate the assumptions used in the open ocean heat budget. In this section, the results from the previous section will be discussed and, whenever possible, comparisons will be made to other relevant studies in this and other regions.

5.1 AASW heat budgets

5.1.1 Surface heat budget

The ice-free heat budget for summer months (Figure 18c) is dominated by input from short wave radiation (Q_{sw}) while the winter budget is dominated by episodic sensible (Q_{sens}) heat losses. Summer values for the daily-averaged short wave radiation can exceed 200 W m^{-2} (Figure 16a) making it the most significant term in the heat budget. The small temperature differences between the atmosphere and AASW at this time result in little contribution from sensible heat exchanges (Figure 16b,e and 18b). During the winter, small zenith angles shorten the length of daylight for the region thereby diminishing the importance of short wave radiation while large temperature differences between the atmosphere and AASW result in sensible heat losses at the air-sea interface that are on the order of 100 to 150 W m^{-2}.

The latent heat flux (Q_{lat}) is generally the least significant term in the heat budget with magnitudes 4 to 10 times smaller than sensible fluxes. Evaporation (and consequentially, latent heat fluxes) is low for the region a result of high, 80% to 90%

relative humidity (Figure 16c). Low evaporative heat losses agree with observations in Cullather et al. [1998] who indicate that the west Antarctic Peninsula region is characterized by net precipitation over evaporation.

Net long wave radiation (Q_{lw}) is predominantly negative throughout the year, indicating that the ocean surface radiates more heat as long wave radiation than it receives. This arises because SST is generally warmer than the atmospheric temperatures throughout the year and because clouds remove part of the incoming radiation. The annual average for long wave radiation is approximately 30 W m^{-2} with modest variations created by changes in cloud cover and air temperature. There is an apparent seasonal trend in long wave radiation (Figure 18a), with winter values being slightly smaller than the summer. This reduction results from ice cover which reduces the area of open water, thus reducing the heat flux.

5.1.2 Total heat budget for surface waters

The time-integrated 1993 heat budget shows AASW losing more heat to the atmosphere than it gains making it a source of heat for the atmosphere (solid line in Figure 23). Winter SST is warm (approximately -2°C) compared to the atmosphere, which is typically colder than -10°C, and winter sensible heat losses are in excess of 100 to 150 W m^{-2}. This result indicates the importance of sea-ice since the large heat loss occurs only through the fraction of the ocean which remains ice-free. Under the assumption that ice acts as a perfect insulator, sensible heat loss would be zero if the shelf were completely ice covered, thus eliminating this source of heat for the atmosphere.

Despite AASW being a heat source for the atmosphere during 1993, there is no evidence in the hydrographic observations for the period showing that AASW experienced any significant cooling between the summer of 1993 and 1994 (Figure 22a). This result agrees with the low net heating between 1993 and 1994 found by

Klinck [1998] which was typically on the order of 5 W m^{-2} (the actual net heating depended on the exact station but was never found to be in excess of 25 W m^{-2}). The integrated 1993 heat budget (solid line in Figure 23) closes to within 25 to 30% of its maximum. Since there is no observed change in the heat content of AASW during the summers of 1993 and 1994 the heat lost must be accounted for by another source. Potential heat replacement processes include horizontal processes, vertical heat fluxes through the permanent pycnocline and heat exchanges between AASW and sea-ice.

Conservative estimates for vertical heat flux from calculations in Klinck [1998] and Smith et al. [1999] are between 5 and 10 W m^{-2}. Including this persistent heat source to AASW in the integration (dashed line in Figure 23) indicates that 5 W m^{-2} is more than enough heat to close the budget and predicts that AASW should gain heat throughout the year but closes the budget to within 10% to 15%. The integrated 1993 budget is closed within 5% of its maximum by including heat exchanges between AASW and the sea-ice with the persistent vertical heat flux calculated above (dotted line in Figure 23). The calculation is performed by prescribing a heat loss of 10 W m^{-2} when the GSFC SMMR/SSMI record indicates the presence of sea ice, an assumption which is later justified by the model results.

The closure of the vertical processes in the above heat budget does not diminish the possibility that horizontal fluxes of heat (and salt) are necessary to completely close the budget; however, they do suggest that much of the local variability observed in AASW can be explained by vertical processes. A further indication of the validity of the budgets can be found by calculating average, net heating between individual 1993 cruises (i.e., the slope of the curves in Figure 23) and comparing them to the observed changes in heat content within AASW calculated in Klinck [1998]. Average heating, cooling rates, from Figure 23 are on the order of ± 50 W m^{-2} and are in agreement with values reported by Klinck [1998].

5.1.3 Validity and limitations of the surface heat flux calculation

The heat fluxes presented in Section 4.1.2 were calculated using data from around Palmer and Faraday Stations located mid-way along the Antarctic Peninsula (Figure 8). The validity of the calculation for the remainder of west Antarctic Peninsula continental shelf remains to be demonstrated. The estimates of sensible and latent heat exchanges are particularly sensitive to atmospheric conditions which may be different offshore whereas short wave radiation is basically estimated from time and geographic location. Klinck and Smith [1995] compare the atmospheric conditions measured at Palmer Station to ship-based measurements recorded during the two month, cruises in fall, 1993 (Table 1). While air temperatures recorded at the station are fairly representative of the conditions over the shelf, wind speed and direction are poorly represented. Smith [1996] compared AWS data from Palmer Station to ASW data from other stations along the coast and found that there was an alongshore gradient in atmospheric temperatures with colder conditions to the south. Given these two results, care must be taken in interpreting heat flux calculations outside of the area surrounding Palmer and Faraday Stations. These results are reasonably accurate for a region within 50 km of Palmer Station (i.e., the arc where GSFC SMMR/SSMI data were extracted in Figure 8). Outside of this region, the results are likely qualitatively correct. The trends in the heat budget, and the relative importance of the individual components most likely stay the same; however, the magnitude of the calculations should change.

5.2 Temporal variability in the winter heat budget

All of the components of the heat budget exhibit variability on time scales of a few days to weeks (Figures 18a-c) which corresponds to time scales associated with the passage of synoptic low pressure systems through Drake Passage. In this section, the effects of one low pressure on the atmospheric conditions and heat fluxes will

be examined as the system passes through Drake Passage during the winter of 1993 (Figure 34).

5.2.1 Temporal variability in the winter sensible heat budget

Mid-winter reversals in temperature and wind direction often coincide with the passage of a low pressure system to the north of the Antarctic Peninsula (Figures 34 and 35). For several days prior to the passage of a synoptic low pressure system, winds are out of the south and atmospheric temperatures are low. During this time, the total heat budget (dominated by sensible fluxes) is characterized by heat losses which are on the order of 100 W m^{-2} (day 240 in Figure 18). When a low pressure system forms to the west of the Peninsula (Figure 34b) atmospheric temperatures increase, winds reverse and sensible heat changes becomes zero (and slightly positive) for several days. After the low pressure system passes the Antarctic Peninsula, air temperature drops, the wind reverse and large heat losses from AASW to the atmosphere occur.

At the time of the passage of the low pressure system (day 230 to 250), the GSFC SMMR/SSMI ice record indicates a 33% reduction in ice cover (Figure 35c). While it is tempting to link the reduction in ice cover to increased atmospheric temperature, and decreased sensible heat fluxes it is unlikely that ice melt is responsible for all of the change. Factors associated with ice motion, not included in this analysis, are also likely to play a role in this change. Winds blowing from the north would tend to pile ice along the coast (increasing A_i), while transporting ice south and out of the domain (decreasing A_i). Thermodynamic effects associated with ice melt will be discussed in more detail in the modeling section of this chapter.

The cumulative effects of the passage of low pressure systems during 1993, and the impact that they have on atmospheric conditions along the Peninsula (Figure 17) indicate that winds from the north (geostrophic flow around a low pressure

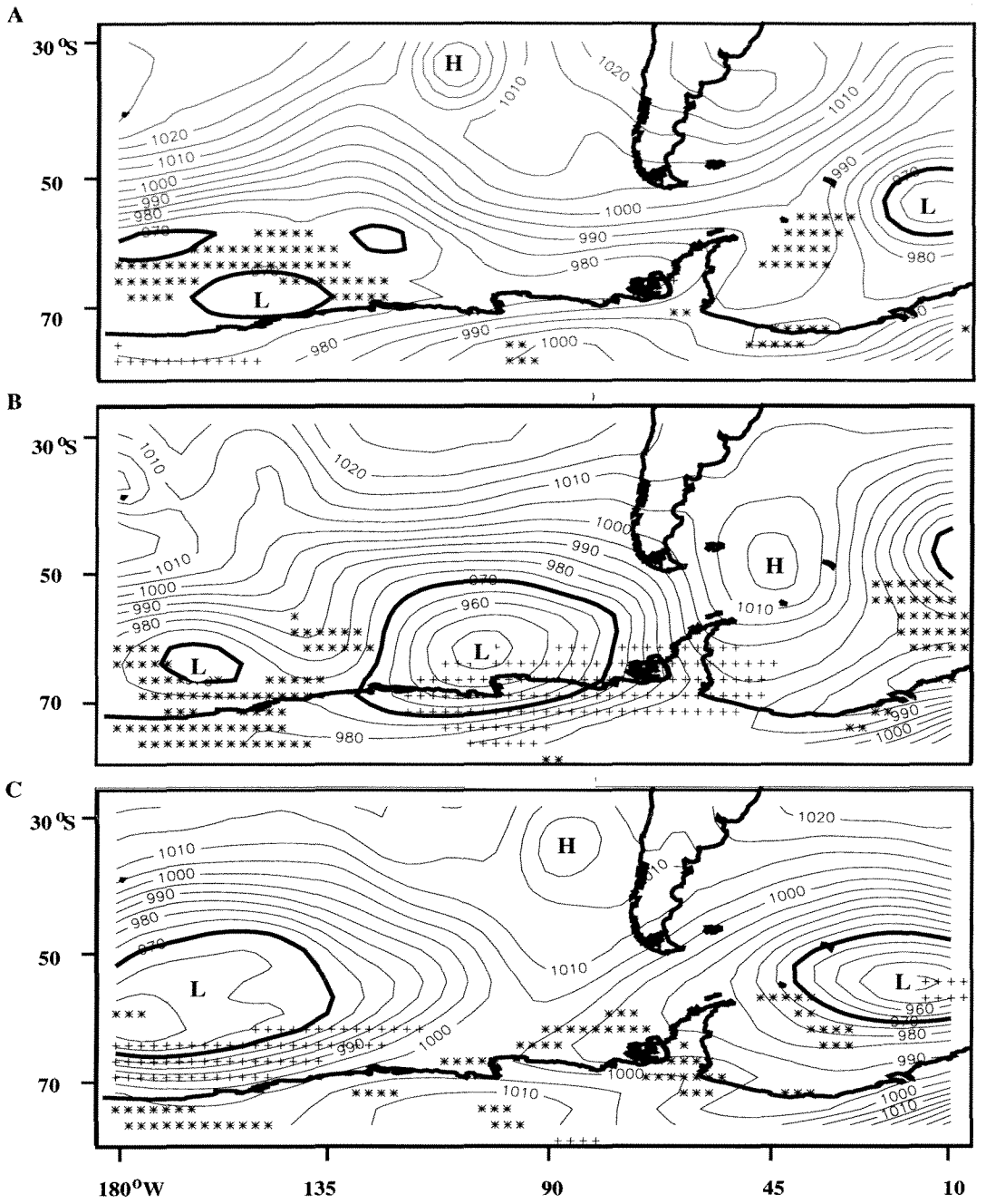

Figure 34. NCEP-derived sea level pressure for Drake Passage and the Southern Ocean (180°W to 30°W) for A) 1 Aug. 1993, B) 5 Aug. 1993 and C) 15 Aug. 1993. NCEP grid cells with temperature anomalies 10°C above and below the monthly mean are indicated with a plus (+) and an asterisks (*), respectively.

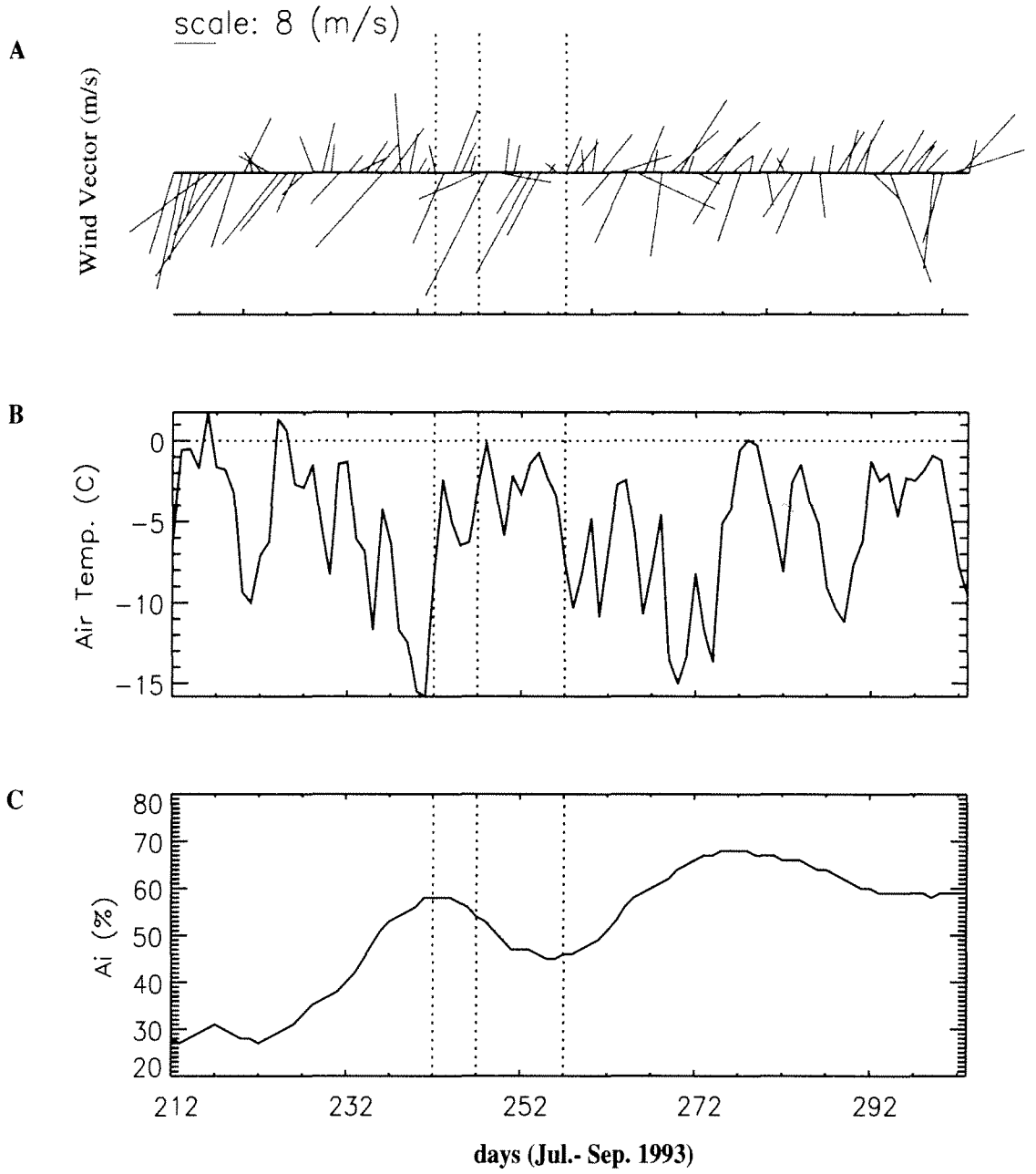

Figure 35. Daily averaged atmospheric and ice conditions for July-September 1993 at Faraday Station. A) Wind vectors with positive x-axis aligning with East, B) Atmospheric temperature and C) GSFC SMMR/SSMI near-Palmer ice area. Days 243, 247 and 257 are indicated with vertical dotted lines and correspond to the days in Figure 34a-c.

system) are associated with warmer conditions. This suggests that low pressure systems in Drake Passage have a significant impact on the overall heat budgets along the Antarctic Peninsula and suggests a link between the frequency and duration of storms and the warm/cold, low/high ice year relationship mentioned in Smith [1996].

5.2.2 The relationship between low pressure systems and interannual variability in the ice cycle

The relationship between storms and ice cover along the shelf to the west of the Antarctic Peninsula has been suggested by Jacobs and Comiso [1993] who relate the extreme low ice year of 1989 to anomalously high winter temperatures, winds from the north and increased storminess. Jacobs and Comiso [1993] do not quantify the "increased storminess" statement; however, it is reasonable to assume that an increase in the frequency, and/or, duration of low pressures in Drake Passage may be associated with increased storm activity.

The idea that synoptic, low pressure systems in Drake Passage result in warmer atmospheric conditions can be extended to include an argument which links the frequency and duration of these low pressure systems to the observed high and low ice years. A year with more frequent and/or longer duration low pressures in Drake Passage would tend to produce milder winters and lower ice coverage. Carleton and Fitch [1993] and Carrasco and Bromwich [1994] studied the relationship between synoptic low pressure systems and the outbreak of mesoscale cyclones after their passage of the Antarctic Peninsula. They indicate that after the passage of synoptic low, cold air outbreaks generate increased cyclonic activity. Van Loon [1991] indicates that the path of the synoptic low pressure systems are such that they either pass the Antarctic Peninsula, or stall in the South Pacific. The storms which stall in the South Pacific tend to produce winters with warmer, average winter temperatures and reduced ice cover.

The monthly NCEP data described in Section 3.1.4 can be used to explore the

link among atmospheric surface pressures, temperature and ice concentration in the vicinity of the Antarctic Continent (Figure 36). Years with anomalously low atmospheric pressures west of the Antarctic Peninsula correspond to years with above average winter temperatures. High and low ice years (Figure 9) correlate to the temperature and pressure anomalies (Figure 36). This relationship is especially apparent in the low ice years in 1983 and 1989 and the high ice year in 1986. Thus, the high/low ice year to cold/warm winter temperature correlation presented in Stammerjohn and Smith [1996] can be extended to include the anomaly in atmospheric surface pressure. All of these relate back to the idea of an Antarctic Circumpolar Wave (ACW) introduced by White and Peterson [1996]. White and Peterson [1996] track atmospheric and oceanic conditions around the Antarctic Continent for several years and find a coupling between the atmospheric temperature, sea level pressure, SST and ice cover. They find a wave, which they call the ACW, in the variable anomalies (departure from a mean) which circles the Continent with a period of 5 to 7 years. The role that low pressure systems play in determining atmospheric temperatures is related to the concept of an ACW and also relates to the observations presented in Jacobs and Comiso [1993] who state that the low ice year of 1989 corresponds to a time of "increased storminess". Results from the numerical model indicate that the direct mechanism for a high or low ice year is an increase or decrease of winter sensible heat flux which is directly related to the atmospheric temperatures.

5.3 Modeled results

5.3.1 Modeled heat fluxes and ice growth

Modeled ice free heat fluxes agree with the heat budgets calculated using atmospheric data from Faraday Station; an expected result, given that the same equations were used in both calculations. The only real difference between the ice free

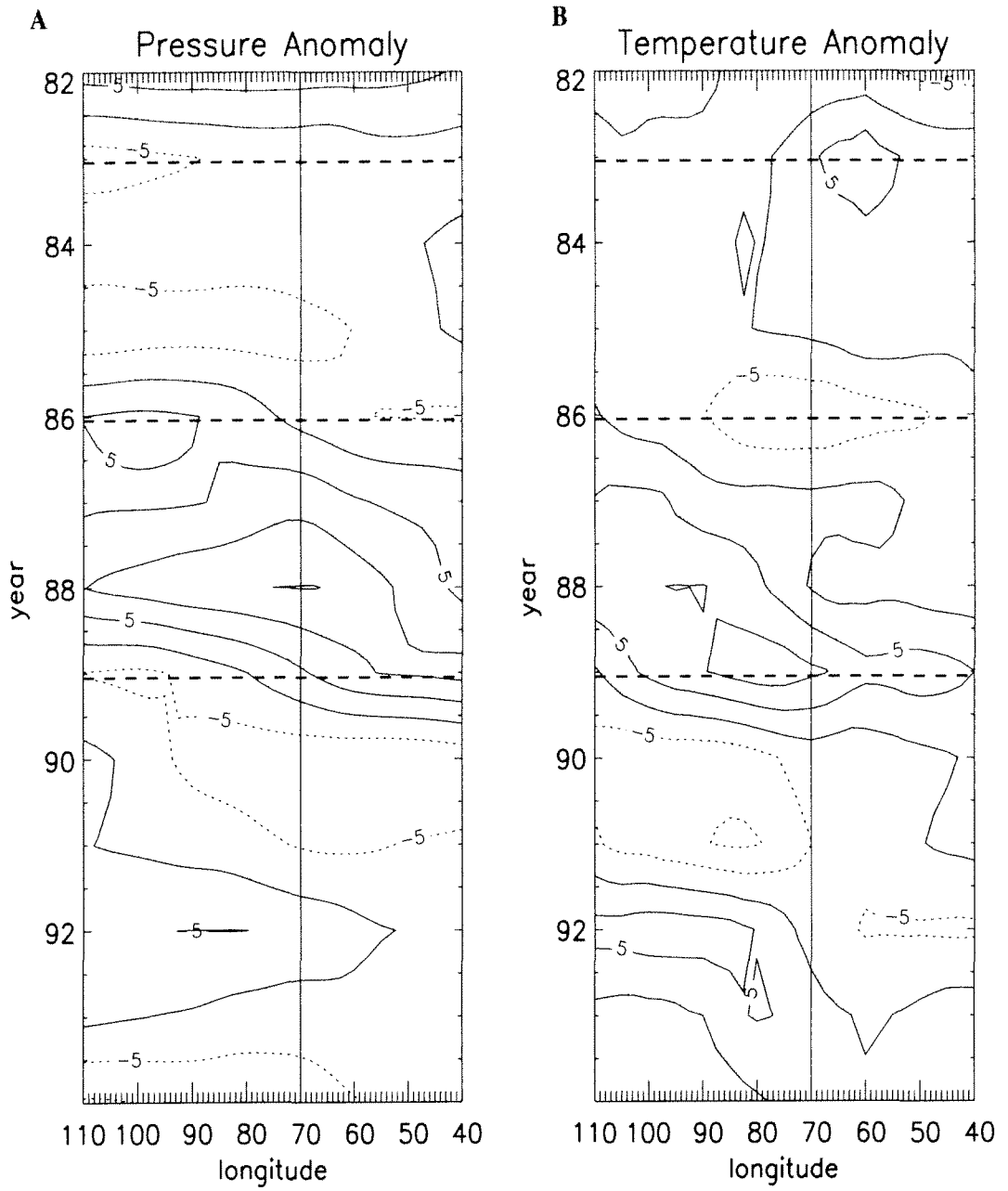

Figure 36. August A) Pressure (mb) and B) Temperature (°C) anomaly for 65°S. The vertical line indicates the location of the west Antarctic Peninsula shelf. Low ice years (1983 and 1989) and a high ice year (1986) are indicated with horizontal dashed lines for reference.

heat fluxes calculated from station data and the simulated heat fluxes is the use of modeled derived SST in the simulation. As already discussed, the overall heat budget is not sensitive to the choice of SST and therefore similarities between the calculations are not surprising.

Modeled heat fluxes between AASW and the ice are on the order of 5 to 10 W m^{-2} while the ice free heat fluxes are generally between 30 and 50 W m^{-2} with maximum heat losses on the order of 100 W m^{-2}. This result is consistent with Arctic simulations [Parkinson and Washington, 1979] where heat fluxes through the 2% of the model which remained ice free were much larger than that through the ice. In this study, through ice heat fluxes were an order of magnitude smaller than those in the ice free regions. The difference between the the results in this study and those of Parkinson and Washington [1979] most likely results from the fact that the west Antarctic Peninsula shelf is generally covered by relatively thin ice as opposed to the thick ice conditions in the Arctic. The averaged through ice heat flux, reported above, excludes the large peak which occurs during the spring when the heat loss from AASW to the ice are calculated to be in excess of 100 W m^{-2}. This large heat flux lasts for a short period of time and drives the rapid melt at the end of the ice cycle.

The result that simulated and calculated sensible heat fluxes were found to be orders of magnitude larger than latent heat fluxes is consistent with results from studies on the Ross Ice Shelf [Stearns and Weidner, 1993]. The low fluxes of latent heat result from the high relative humidities observed in the region (Figure 16c).

5.4 Modeled ice cycle

The simulated ice cycle reproduces well the GSFC SMMR/SSMI record capturing key features such as the timing of initial growth and the rapid spring melt (Figure 25a). The modeled ice cycle also reproduces much of the higher frequency variability

observed in the ice field which is most likely associated with the passage of storms through Drake Passage. The model results agree with the observations from the open-ocean, heat flux calculation which indicate that the timing of the ice cycle is largely determined by net solar radiation while the ice extent is determined by sensible heat flux driven by atmospheric temperatures.

Results from the model also suggest that modified-UCDW on the shelf influences overall ice thickness. Once AASW stratification is eroded (due to surface mixing, cooling and brine rejection), heat which is diffused vertically through the permanent pycnocline is available to melt the ice from underneath. Increasing the heat in the sub-pycnocline waters increases the overall heat available to AASW and reduces the overall ice thickness (Figure 31a,c). Similarly, increasing mixing reduces ice concentration (Figure 31b,d). As Martinson [1990] found for the Weddell Sea, this latter result indicates the importance of the role of the double diffusive instability in the balance of heat and salt in AASW. The process increases the flux of heat to AASW without greatly increasing the exchange of salt (Figure 32).

The simulations demonstrate that the two dominate terms in (23) are ice growth in the ice-free portion of the model (driven by sensible heat loss) and ice melt at the ice-ocean interface. These terms determines the net ice growth for a given period of time. The mid-winter reduction in the GSFC SMMR/SSMI ice area (associated with the passage of a low pressure system through Drake Passage and discussed in the previous section) is reproduced by the model (Figure 25a) suggesting that some of the reduction results from thermodynamic effects. When atmospheric temperature is warm, sensible heat losses from AASW to the atmosphere are reduced thus shutting off ice growth in the portion of the model which remains ice free. When ice is not being formed in the open ocean, ice melt at the ice-ocean interface drives net ice melt (see day 240 in Figure 26a). While this argument does not rule out the effect of motion on ice reduction, it does suggest that thermodynamics is important.

5.5 Modeled surface water hydrography

The model reproduces typical temperature and salinity ranges observed in the hydrography as well as several key hydrographic features of the system such as *mld* and the top of the permanent pycnocline. In this section, these features will be discussed.

5.5.1 Surface mixed layer and mixed layer depths

The depth of the mixed layer, and the hydrographic character of the upper water column, results from complex interaction between buoyancy forcing associated with surface thermodynamics (including ice processes) and momentum fluxes associated with wind and ice induced motion. Surface cooling during the fall, and the subsequent brine rejection associated with ice formation, drive winter *mld's* to the depth of the permanent pycnocline (140 to 150 m). In addition to the buoyancy driven convective mixing, momentum flux under the ice is large and these combine to produce large turbulent fluxes (Figure 29) which also deepen the mixed layer.

The absorption of short wave radiation through open leads during the spring drives a large heat flux to AASW which melts the ice over a period of a few weeks. This modeled, rapid ice melt, reproduces observations presented in Stammerjohn and Smith [1996] and is a strong indication that the input of solar radiation dominates the timing of the ice cycle. Ice melt generates a thin layer of fresh water at the surface of the model. Once all of the ice has melted, surface heating warms the surface layer increasing the surface stratification and generating a distinct seasonal pycnocline. It is between this seasonal pycnocline and the top of the permanent pycnocline where the distinct temperature minimum of WW is found.

Models that use the free drift equations (Section 3.4.4) for ice velocity tend to overestimate the *mld* because of excessive ice velocity. The free-drift equations lack internal pressure terms (i.e., rheology) which results from horizontal gradients in

the ice thicknesses or contact with land masses.

Modeled ice velocities in this study are typically 0.5 to 0.75 m s^{-1} which are higher than one would expected and a balance is established in (34) between the drag at the ice-water and atmosphere-ice interfaces ($\tau_{iw}^{(x,y)}$) and air-ice ($\tau_{ai}^{(x,y)}$), respectively). This analysis is not shown, but is consistent with results reported in Ikeda [1989]. Despite this limitation of using (34), the modeled depths of the convective, winter mixed layer agree well with observations (Figure 28) indicating that the higher than expected ice velocities do not invalidate the solution and indicates that the depth of the winter mixed layer is largely determined by surface buoyancy effects and the position of the permanent pycnocline. The mixing under the ice is sufficient to eliminate any stratification from mid-winter ice melt.

The model fails to reproduce surface salinities which are fresher that 33.2 observed during the fall 1993 cruise [Smith et al., 1999] even after ice melt. Smith et al. [1999] indicate that stations occupied where the fresh water were sampled was near near Marguerite Bay most likely originates as glacial melt. The modeled salinity changes are consistent with the formation and melting of the amount of ice produced during the simulation and the prescribed precipitation.

5.5.2 The depth of the permanent pycnocline

During the winter, the permanent pycnocline is defined by the depth of the mixed layer and is generally found between the depths of 140 to 150 m (Figure 28a). As discussed in the previous section, winter AASW hydrography is characterized by well mixed conditions and no stratification. During the spring and summer, surface warming and fresh water input results in the formation of a seasonal pycnocline (Figure 4a). The seasonal pycnocline persists through the fall when intense fall and winter mixing (Figure 29a), once again eliminates surface stratification, and the seasonal pycnocline.

The formation of the seasonal pycnocline plays an important role in the position of the permanent pycnocline. When stratification exists in the upper 100 m of the water column, heat and salt fluxes from beneath the permanent pycnocline are trapped at the depth of WW warming it and increasing its salinity. The trapping of heat and salt appears as a slow lifting of the permanent pycnocline which occurs throughout the simulation while the surface of the model is stratified. Once the surface stratification is eliminated, the heat stored in WW is released for mixing with surface waters; thus, a direct link between the heat flux though the permanent pycnocline and the atmosphere/ice interfaces is established. This transfer is further enhanced by the intense winter mixing.

5.5.3 Modified-CDW and double diffusion

The warm, salty character of the sub-pycnocline water on the shelf differentiates the shelf to the west of the Antarctic Peninsula from other Antarctic shelf systems [Hofmann and Klinck, 1998]. As discussed in the previous section, the heat flux through the permanent pycnocline may play an important role in the hydrographic character of WW and in the formation of ice. While the timing of the ice cycle appears to be determined by input of solar radiation (in particular short wave radiation) the extent of winter ice is determined by a delicate balance between melting at the base of the ice and ice formation at the ice-ocean interface. To a large extent, atmospheric conditions control this balance; however, heat fluxes through the permanent pycnocline definitely impacts growth at the ice ocean interface and therefore affect net ice production. The model indicates that heat fluxes through the permanent pycnocline are typically 10 W m^{-2} which is also the average under ice heating suggesting that the heat supplied from beneath the permanent pycnocline drives winter ice melt, when atmospheric conditions would favor growth.

For model simulations with warm sub-pycnocline temperature (i.e., consistent

with pure UCDW) the winter ice cover was reduced by nearly 50% while the model formed more ice for simulations with reduced deep temperatures. Changes in the sub-pycnocline hydrography affect the ice field primary after day 170 due to the presence of the seasonal pycnocline (Figure 28).

Double diffusion increases the flux of heat (primarily) and salt (slightly) through the permanent pycnocline to AASW which determining the character of WW. The importance of double diffusion to the overall heat budget is first presented in Smith et al., [1999] and Klinck [1998] and explored in this study through its implementation in the numerical model. The results indicate that the process is important in determining the overall thickness of ice during maximum ice extent (Figure 31b,c) and the hydrography of WW (Figure 32). When double diffusion is not included in the model, WW does not warm sufficiently; however, if the background diffusion is increased to compensate for the under-heating then WW becomes too warm and salty (Figure 32). This result indicates that the differential transfer of heat and salt (more heat than salt) is important in determining the character of AASW, in particular WW.

5.6 Trends observed from the 16 year model run

The long record of atmospheric data from Faraday was used to force the model over a 16 year period which coincides with the GSFC SMMR/SSMI ice area time series (Figure 9b). Modeled trends in the ice concentrations and the hydrographic response and mixed layer structure are discussed in this section.

5.6.1 Modeled ice cycle

The winter ice cover to the west of the Antarctic Peninsula is characterized by an inter-annual variability of high and low ice years which correlates to atmospheric conditions (Figure 9) [Jacobs and Comiso, 1993; Smith et al., 1996; Stammerjohn

and Smith, 1996 and Stammerjohn and Smith, 1997]. In Section 4.3.4 the one dimensional model is forced with atmospheric conditions from Faraday and the resulting ice cycle reproduces this high/low ice cycle fairly well (Figure 33). Of particular interest is the model's ability to reproduce one of the highest and lowest ice years on record (1987 and 1989, respectively). In addition to the extremes, the model was able to reproduce many of the observed trends such as the consecutive high ice years of 1979-1982, which were immediately followed by three low ice years from 1983 to 1985.

Given the vertical only character of the model used in the study, and its ability to reproduce many of the observed trends in the ice field, these results support the findings of Smith [1996] who suggests an atmospheric (that is, thermodynamic) control on the ice cover. This conclusion is also supported by the model results which suggest that the primary mechanism for winter ice growth is sensible heat loss during the winter months which is primarily driven by temperature differences between the atmosphere and the ocean. It also supports the concept of the ACW which may account for the observed inter-annual variability in atmospheric conditions along the Antarctic Peninsula.

While the model does produce 1980 as a high ice year, it fails to indicate it as the highest ice on record (Figures 9b and 33a). One possible explanation for this mismatch is the exclusion of horizontal processes in the model and the numerical treatment of the sub-pycnocline water which are nudged to hydrographic conditions imposed from 1993 data. Given the persistent character of sub-pycnocline waters [Hofmann et al., 1996], over decadal time scales, the use of 1993 data throughout the simulation is a reasonable first assumption. However, the sensitivity of the modeled ice cover to changes in the parameterization of double diffusion, and the temperature of the modified-UCDW (Section 4.3.3) suggests that the difference in the modeled ice cover could be explained by changed temperature of the sub-pycnocline waters.

The data record does not contain detailed observations of the shelf waters for 1980; however, if the waters were colder than the average temperature used in the model, the difference would be explained.

5.6.2 Hydrographic response

The trends in the ice field which were discussed in the previous section, and the relationship between the ice and the atmosphere have been understood for several years. Unfortunately, the lack of a long time series of high quality hydrographic data for the region has limited investigations to the atmosphere and the ice cycle while the ocean's role has not been included. This analysis based on an observation of a model permits the ocean's role to be investigated.

Of particular interest from the model results are the depth of the mixed layer and the permanent pycnocline. A time series of these parameters are available from the hydrographic data but are important in understanding the system's physics and biology. Model results indicate that the warm/cold to low/high ice year linkage can be extended to include shallow/deep winter mixed layers (Figure 33a). The depth of the permanent pycnocline was generally found 40 to 50 m deeper during high ice years as compared to low ice years.

Additionally, spring *mld* was found to be shallower and more stable following a high ice year. This results from an increased input of fresh water from ice melt. Results also suggest that years following high ice cover would favor stability in the surface waters and increase primary production.

While the results from the sixteen year simulation are interesting, they must be interpreted with caution. The model used for these simulations is only a vertical model and neglects horizontal processes on ice dynamics and thermodynamics. The low ice years, which appear to coincide with years of increased low pressure activity in Drake Passage (Figure 36) would also be years when prevailing, geostrophic winds

from the north would compress ice against the coast, closing leads and producing thicker ice cover. These dynamics oppose the thermodynamic tendency increased atmospheric temperatures to reduce overall ice cover. A full investigation of horizontal processes would require a more elaborate numerical model capable of simulating ice convergence/divergence.

CHAPTER 6
SUMMARY AND CONCLUSIONS

The oceanic and atmospheric observations combined from ship and station observations near Palmer Station provide an excellent source of data for the investigation of air/ice/sea interactions along the region to the west of the Antarctic Peninsula. These data also provide the basis for the development of numerical models which are used to further investigate the physical processes in the system, its temporal variability and the oceanic response to atmospheric and ice driven surface buoyancy forcing. The observations and the results from the simulations are summarized in this chapter.

6.1 Hydrographic observations

Hydrography observations along the west Antarctic Peninsula are used to characterize the shelf waters as consisting of a two layer system. AASW occupies the upper 100 to 200 m of the water column and exhibits hydrographic variability on time scales consistent with atmospheric heating, cooling and ice related buoyancy forcing. A distinct permanent pycnocline separates AASW from a deeper layer of water with oceanic origin originating in the ACC as UCDW. This lower layer of water has relatively warm temperatures ($> 1.4°C$) and high salinities (> 34.6 psu) and exhibits very little variability on seasonal, annual and decadal time scales.

Klinck [1998] and Smith et al.[1999] propose that the deep, modified-UCDW forms as pure UCDW, from the ACC, intrudes on the the shelf and diffuses heat and salt vertically through the permanent pycnocline to the cooler, fresher AASW (WW) above. The authors test a first order balance of horizontal and vertical transfer of heat and salt and find that the balance is consistent with reasonable oceanic parameters. Calculations presented in this study support this finding and suggest

that the hydrographic character of the sub-pycnocline waters can be maintained with horizontal eddy diffusion coefficients on the order of 10 m^2 s^{-1} which balance vertical diffusive losses from modified-UCDW to AASW (WW).

Simple double diffusive calculations based on $\Delta T^{\frac{4}{3}}$ models and model results indicate that vertical diffusion of heat (mainly) and salt (slightly) are enhanced by double diffusion. Model results suggest that double diffusion accounts for at least 50% (5 to 10 W m^{-2}) of the total heat transferred through the permanent pycnocline while the prescribed background diffusion accounts for the rest. Furthermore, double diffusion allows for a differential vertical transfer of heat and salt which appears to be necessary for the proper hydrographic character in the bottom portion of AASW (WW).

6.2 Vertical and horizontal fluxes of heat and salt

The atmospheric data from the vicinity of Palmer Station are used to estimate surface rates of heating and to rank the importance of individual terms in the heat overall budget. Using these data, net atmospheric heating, and cooling, rates between the 1993 Palmer-LTER cruises are estimated to be $\pm$ 50 W m^{-2}. These estimates agree with calculations presented in Klinck [1998] who used measured oceanic temperatures to estimate the required heating, and cooling, necessary to produce the observed hydrographic changes between the same cruises.

The results from the open-ocean heat budget (Section 4.1.2) indicate overall exchanges of heat at the atmosphere/ice/ocean interface are on the order of $\pm$ 150 to 200 W m^{-2}. The net heat budget for 1993, estimated by integrating the time series of calculated heat fluxes, balances giving a net heating near zero W m^{-2}. This net result near zero requires the assumption that heating from below the permanent pycnocline is a persistent process throughout the year and that, on average, 10 W m^{-2} of heat is lost from AASW to sea ice when sea ice is present. These two

assumptions are supported by the results of the model analysis.

Given the magnitude of the open-ocean, atmospheric heat fluxes, ($\sim \pm$ 150 to 200 W m^{-2}) and the closure of the integrated budget, two general conclusions can be made: 1.) heat fluxes at the atmosphere/ocean interface account for most of the vertical exchanges of heat, and 2.) local atmospheric conditions along the west Antarctic Peninsula account for much of the observed variability in the shelf's hydrography. The ability of the vertical model to reproduce the high/low ice cycle means that local atmospheric conditions control ice processes along the region to some extent. This result is consistent with the work of Smith et al. [1996] and Stammerjohn and Smith [1996] who link the high/low ice years along the Peninsula to cold/warm atmospheric conditions.

During the summer months, the surface heat flux is dominated by incoming short wave radiation on the order of 200 W m^{-2} and occurs at a time when sensible heat losses are small because atmospheric and oceanic temperatures are similar. During the fall and through the winter, atmospheric temperatures can reach lows below -15°C while SST is clamped by the freezing point ($T_f \sim$ -2°C). The large differential between atmospheric and oceanic temperatures (with the atmosphere being cooler) leads to high rates of sensible heat loss and dominates the winter heat budget. Open-ocean, wintertime, sensible heat losses can be in excess of 100 to 150 W m^{-2}, producing ice formation in the portion of the ocean which remains open (i.e. leads).

Other terms in the surface heat budget play a less significant role in the overall heating. Net long wave radiation is on the order of 30 W m^{-2} and is a persistent throughout the year; high values of relative humidity ($\sim$ 90%) diminishes the importance of latent heating in the region. Latent heating is typically one tenth that of the sensible heating.

6.3 Momentum fluxes, vertical mixing and the depth of the mixed layer

Mixed layer depths from observations and those from the model are consistent with each other (Figure 28). While mixed layer depths from hydrographic observations give an accurate, detailed account of the surface density structure during the times of the observations, the model provides a tool for evaluating the physical processes which determine the depth of the mixed layer and provides insight into the time evolution of characteristics within AASW. Model results indicate that ice formation, brine rejection, surface cooling and ice driven mixing produce well mixed hydrographic conditions which extend to the bottom of AASW (150 to 200 m).

Well mixed conditions persist throughout the winter until the ice retreats during the spring melt. During this retreat, a thin layer of fresh water forms at the surface of model which warms and stabilizes the surface. Beneath this layer, a seasonal pycnocline forms separating the wind mixed layer at the surface (top 10 to 20 m) from the temperature minimum found at depth indicating the position of the bottom of AASW (WW). This seasonal pycnocline forms a density barrier to the vertical mixing of heat and salt, trapping the heat and salt which is mixed from below the permanent pycnocline in the WW. This heating through the permanent pycnocline slowly erodes the hydrographic character of WW resulting in a lifting of the permanent pycnocline.

Stratification within AASW persists through the summer until the subsequent fall when surface cooling and wind mixing drives the mixed layer deeper. The mixed layer is reset to its winter depths when ice forms during the next winter. As the winter mixed layer is reset, it erodes the heat stored in WW which was trapped by the existence of the seasonal pycnocline. An important period of time in the model simulations occurs when the surface mixed layer is driven back to the depth of the permanent pycnocline. At this time, the stratification within AASW is eliminated

and heat fluxes from modified-UCDW are no longer impeded from the surface and become available to the atmosphere (in the portion of the ocean which remains ice free) and to the ice. The results from the model indicate that when stratification within AASW is eliminated, the under ice growth rate switches from a growth term, to a persistent ice loss term slowing the overall ice growth.

Within AASW, eddy diffusion coefficients are quite large and range from 0.01 to 0.001 m s^{-2} with the higher coefficients occurring in the winter under the influence of ice formation and ice driven mixing. Diffusion coefficients within the permanent pycnocline are typically on the order of 1×10^{-4} $m^2 s^{-1}$ and are enhanced by double diffusion.

6.4 Ice processes

The timing of the ice cycle is largely determined by the input of short wave radiation while the extent of the ice at winter maximum (i.e., thickness and/or concentration) is determined by sensible heat losses at the air/ocean interface. These sensible heat losses drive freezing rates in the open ocean which can exceed several centimeters per day. The primary balance in the ice growth equation is between growth at open ocean and ice melt at the ice-ocean interface. The balance between these two processes determines whether or not ice is forming or melting.

The presence of warm, oceanic water beneath the permanent pycnocline determines the thickness of the ice at maximum ice extent. It does not, however, seem to affect the timing of the onset of ice formation or spring melt. Likewise, the parameterization of heat fluxes through the permanent pycnocline is significant in determining the overall extent of the winter ice thickness. Model results from sensitivity tests indicate that ice cover is reduced by as much as 50% when considering double diffusion in the vertical transfer of heat as compared to when it is not included.

6.5 Temporal variability and winter storms

An interesting result is that ice growth can be stopped, and reversed (ice melt), in mid-winter by large temperature reversals, which occur on time scales coincident with the passage of synoptic low pressure systems through Drake Passage, as seen in atmospheric data collected at Palmer Station. Several mid-winter temperature reversals are seen in the atmospheric data collected at Palmer Station (Figure 16b). The response in the resulting heat budgets and ice growth rates are also observed (Figures 18c and 26b). During several of these mid-winter episodes where atmospheric temperatures warm by 15 to 20°C and ice cover in the model is reduced by up to 40%.

The occurance along the west Antarctic Peninsula of warm (cold) winters low (high) ice cover [Smith et al., 1996] is linked to the frequency and duration of synoptic low pressure systems in and around Drake Passage. An investigation using data from the NCAR/NCEP re-analysis project suggests that a suite of coupled anomalies (i.e., atmospheric pressure at sea level, atmospheric temperatures, SST and ice cover), termed the ACW, manifests itself along the west Antarctic Peninsula and supports concept of high/low ice years.

6.6 Relevance to other studies and concluding remarks

Biologists who study the waters to the west of the Antarctic Peninsula are interested in the sometimes complex density structures which form within AASW under the competing forces of wind mixing, ice driven buoyancy forcing, surface heating and cooling. These forces act to determine the hydrographic character of the surface waters along the west Antarctic Peninsula. Understanding these processes is crucial to understanding the biology for the region.

During the winter, brine rejection, surface cooling and intense wind and ice driven mixing combine to drive deep well mixed layers within AASW. These con-

ditions do not favor biological organisms which have little, or no ability, to control their position within the water column. Conversely, the shallow, stable surface mixed layers which form in the spring during ice melt are conditions which highly favor large blooms of phytoplankton. These concentrations of phytoplankton are the fundamental basis for the region's food web.

The presence of modified-UCDW on the shelf, introduces a unique source of heat and salt to the shelf waters. This heat source is available to interact with the ice and atmosphere along the west Antarctic Peninsula and has potential impact on both biological and atmospheric sciences.

The results from this study are intended to form the basis for future work in the the region. The processes investigated here should lend insight into the development of two- and three-dimensional ice-ocean modeling studies which will be able to directly investigate horizontal processes and how they affect ice cover and biological processes along the west Antarctic Peninsula.

REFERENCES

Blumberg, A. F., and G. L. Mellor, A description of a three-dimensional coastal ocean model, Heaps, N. S. (editor), *Coastal and Estuarine Science 4: Three-Dimensional Coastal Ocean Models.* American Geophysical Union, Washington, D.C., 1987.

Capella, J. E., Circulation and temperature effects on the development and distribution of the eggs and larvae of the Antarctic krill, *Euphausia superba*: A modeling study, Ph.D. thesis, Texas A&M University, 162 pp., 1989.

Carelton A., and M. Fitch, Synoptic aspects of Antarctic mesocyclones, *J. Geophys. Res.*, *98*, 12,997–13,018, 1993.

Carrasco, J. F., and D. H. Bromwich, Climatological aspects of mesoscale cyclogenesis over the Ross Sea and Ross Ice Shelf regions of Antarctica, *Mon. Wea. Rev.*, *122*, 2405–2425, 1994.

Cavalieri D. J., Claire L. P., P. Gloersen, and H. J. Zwally, Arctic and Antarctic sea ice concentrations from multichannel passive-microwave satellite data sets: October 1978 - September 1995, Technical Report 104647, NASA, Goddard Space Flight Center, Washington, D.C., 17 pp., 1997.

Clowes, A. I. J., Hydrography of the Bransfield Strait, *Discovery Reports*, *9*, 1–64, 1934.

Comiso, J. C., D. J. Cavalieri, C. L. Parkinson, and P. Gloersen, Passive microwave algorithms for sea ice concentration: a comparison of two techniques, *Remote Sens. Environ.*, *60*, 375–384, 1997.

Cullather, R. I., D. H. Bromwich, and M. L. Van Woert, Spatial and temporal

variability of Antarctic precipitation from atmospheric methods, *J. of Climate*, *11*, 334–367, 1998.

Everson, I., and D. G. M. Miller, Krill mesoscale distribution and abundance: results and implications of research during the BIOMASS programme, El-Sayed, S. Z. (editor), *Southern Ocean Ecology: the BIOMASS prespective.* Cambridge University Press, Cambridge, pp. 129-144, 1994.

FRAM Group, An eddy-resolving model of the Southern Ocean, *EOS*, *72*, 169, 174–175, 1991.

Fujino, K., E. L. Lewis, and R. G. Perkins, The freezing point of seawater at pressures up to 100 bars, *J. Geophys. Res.*, *79*, 1792–1797, 1974.

Gordon, A. L., and W. D. Nowlin, Jr., The basin waters of the Bransfield Strait, *J. Phys. Oceanogr.*, *8*, 258–264, 1978.

Häkkinen, S., and G. L. Mellor, One hundred years of arctic ice cover variation as simulated by a one-dimensional, ice-ocean model, *J. Geophys. Res.*, *95*, 15,959–15,969, 1990.

Hibler, W. D., III., A dynamic thermodynamic sea ice model, *J. Phys. Oceanogr.*, *9*, 815–846, 1979.

Hofmann, E. E., and J. M. Klinck, Hydrography and circulation of the Antarctic continental shelves: 150°E eastward to the Greenwich Meridian, Robinson, A. R. and K. H. Brink (editors), *The Sea, The Global Coastal Ocean, Regioanl Studies and Synthesis*, Volume *11*, 1998.

Hofmann, E. E., J. M. Klinck, C. M. Lascara, and D. A. Smith, Water mass distribution and circulation west of the Antarctic Peninsula, Ross, R. M., E. E.

Hofmann and L. B. Quetin (editors), *Foundations for Ecological Research West of the Antarctic Peninsula.* American Geophysical Union, 1996.

Huntley, M. E., D. M. Karl, P. P. Niiler, and O. Holm-Hansen, Research on Antarctic coastal ecosystem rates (RACER): an interdisciplinary field experiment, *Deep Sea Res.*, *38*, 911–941, 1991.

Ikeda, M., A coupled ice-ocean mixed layer model of the marginal ice zone responding to wind forcing, *J. Geophys. Res.*, *94*, 9699–9709, 1989.

Jacobs, S. S., and J. C. Comiso, A recent sea-ice retreat west of the Antarctic Peninsula, *Geophys. Res. Let.*, *20*, 1171–1174, 1993.

Jones, P. D., and D. W. S. Limbert, *A data bank of Antarctic surface temperature and pressure data, Office of Energy Research*, Office of Basic Energy Sciences, Carbon Dioxide Research Division, Washington, D. C., 1987.

Kamph, J., and J. O. Backhaus, Shallow, brine-driven free convection in polar oceans: Nonhydrostatic numerical process studies. *J. Geophys. Res.*, *103*, 5577–5594, 1998.

Kalnay, E., M. Kanamitsu, R. Kistler, W. Collins, D. Deaven, L. Gandin, M. Iredell, S. Saha, G. White, J. Woollen, Y. Zhu, , A. Leetmaa, R. Reynolds, M. Chelliah, W. Ebisuzaki, W. Higgins, J. Janowiak, K. C. Mo, C. Ropelewski, J. Wang, R. Jenne, and D. Joseph, The NCEP/NCAR 40-year reanalysis project, *Bull. of the Amer. Meteorol. Soc.*, 1996.

Kantha L. H., and C. A. Clayson, An improved mixed layer model for geophysical applications, *J. Geophys. Res.*, *99*, 25,235–25,266, 1994.

Kantha, L. H., and G. L. Mellor, A two-dimensional coupled ice-ocean model of the

Bering Sea marginal ice zone, *J. Geophys. Res.*, *94*, 10,921–10,935, 1989.

Kelly, D., Effective diffusivities within oceanic thermohaline staircases, *J. Geophys. Res.*, *89*, 10,484–10,488, 1984.

Klinck, J. M., Heat and salt changes on the continental shelf west of the Antarctic Peninsula between January 1993 and January 1994, *J. Geophys. Res.*, 7617 - 7636, 1998.

Klinck, J. M., and D. A. Smith, Palmer lter: Comparison of meterological observations from RV N.B. Palmer to those at Palmer Staton, *Antarctic J. of the U. S*, 1995.

Klinck, J. M., R. C. Smith, and D. Menzies, Hydrographic data collected aboard *RV Polar Duke* August-September 1993, Technical Report 94-01, Center for Coastal Physical Oceanography, Old Dominion University, Norfolk, VA, 265 pp., 1994.

Laevastu, T., Factors affecting the temperature of the surface layer of the sea, *Comment. Phys. Math.*, *25*, 1, 1960.

Large W. G., J. C. McWilliams, and S. Doney, Oceanic vertical mixing: A review and model with a nonlocal boundary layer parameterization, *Rev. of Geophys.*, *99*, 25,235–25,266, 1994.

Lascara, C. M., R. C. Smith, D. Menzies, and K. S. Baker, Hydrographic data collected aboard *RV Polar Duke* January-February 1993, Technical Report 93-02, Center for Coastal Physical Oceanography, Old Dominion University, Norfolk, VA, 265 pp., 1993a.

Lascara, C. M., R. C. Smith, D. Menzies, and K. S. Baker, Hydrographic data col-

lected aboard *RV Polar Duke* november 1991, Technical Report 93-01,, Center for Coastal Physical Oceanography, Old Dominion University, Norfolk, VA, 95 pp., 1993b.

Lemke, P., A coupled one-dimensional sea ice-ocean model, *J. Geophys. Res.*, *92*, 13,164–13,172, 1987.

Lemke, P., W. B. Owens, and W. D. Hibbler, III, A coupled sea ice-mixed layer-pycnocline model for the Weddell Sea, *J. Geophys. Res.*, *95*, 9513–9525, 1990.

Marmorino, G. O., and D. R. Caldwell, Heat and salt transport through a diffusive thermohaline interface, *Deep Sea Res.*, *23*, 59–67, 1976.

Marr, J. W. S., The natural history and geography of the Antarctic krill (*Euphausia superba* Dana), *Discovery Reports*, *32*, 33–464, 1962.

Martinson, D. G., Evolution of the Southern Ocean winter mixed layer and sea ice: open ocean deepwater formation and ventilation, *J. Geophys. Res.*, *95*, 11,641–11,654, 1990.

Maykut, G. A., and N. Untersteiner, Numerical prediction of the thermodynamic response of Arctic sea ice to environmental changes, Technical Report RM-60093-PR, The Rand Corporation, Santa Monica, CA, 1969.

Mellor, G. L., *User's guide for a three-dimensional, primitive equation, numerical ocean model.* Princeton University: Report AOS Program, Princeton NJ 08540, 1993.

Mellor, G. L., and L. H. Kantha, An ice-ocean coupled model, *J. Geophys. Res.*, *94*, 10,937–10,954, 1989.

Mellor, G. L., and T. Yamada, A hierarchy of turbulence closure models for planetary boundary layers, *J. Atmos. Sci.*, *31*, 1791–1896, 1974.

Mellor, G. L., and T. Yamada, Development of a turbulence closure model for geophysical fluid problems, *Rev. of Geophys. Space Phys.*, *20*, 851–875, 1982.

Mosby, H., The Waters of the Atlantic Antarctic Ocean. Scientific Results of the Norwegian Antarctic Exediton 1927-1928 *11*, 1-131.

Niiler, P. P., A. Amos, and J. H. Hu, Water masses and 200 m relative geostrophic circulation in the western Bransfield Strait region, *Deep Sea Res.*, *38*, 943–959, 1991.

Niiler, P. P., J. Illeman, and J. H. Hu, RACER: Lagrangian drifter observations of surface circulation in the Gerlache and Bransfield Straits, *Antarctic J. of the U. S.*, *25*, 134–137, 1990.

Nowlin, W. D., Jr., and M. Clifford, The kinematic and thermohaline zonation of the Antarctic Circumpolar Current at Drake Passage, *J. Mar. Res.*, *40*, 481–507, 1982.

Parkinson, C. L., and W. M. Washington, A large-scale numerical model of sea ice, *J. Geophys. Res.*, *84*, 311-336, 1979.

Semtner, A. J., Jr., *An oceanic general circulation model with bottom topography, numerical simulation of weather and climate.* Technical Report 9, Department of Meteorology, University of California, 1974.

Semtner, A. J., Jr., A model for the thermodynamic growth of sea ice in numerical investigations of climate, *J. Phys. Oceanogr.*, *6*, 379–389, 1976.

Sievers, H. A., and W. D. Nowlin Jr., The stratification and water masses at Drake Passage, *J. Geophys. Res.*, *89*, 10,489–10,514, 1984.

Smith, D. A., E. E. Hofmann, J. M. Klinck, and C. M. Lascara, Hydrography and circulation of the West Antarctic Peninsula shelf, *Deep Sea Res.*, *46*, 925-949, 1999.

Smith, D. A., R. A. Locarnini, B. L. Lipphardt, Jr., and E. E. Hofmann, Hydrographic data collected aboard *RV Nathaniel B. Palmer* March-May 1993, Technical Report 93-04,, Center for Coastal Physical Oceanography, Old Dominion University, Norfolk, VA, 265 pp., 1993a.

Smith, D. A., R. C. Smith, and D. Menzies, Oceanographic data collected aboard *RV Nathaniel B. Palmer* March-May 1993, Technical Report 93-05, Center for Coastal Physical Oceanography, Old Dominion University, Norfolk, VA, 265 pp., 1993b.

Smith, R. C., K. Baker, W. Fraser, E. Hofmann, D. Hofmann, D. Karl, J. Klinck, L. Quetin, B. Prézelin, R. Ross, W. Trivelpiece, and M. Vernet, The Palmer LTER: A Long-Term Ecological Research Program at Palmer Station, Antarctica, *Oceanography*, *8*, 77–86, 1995.

Smith, R. C., S. E. Stammerjohn, and K. S. Baker, Surface air temperature variations in the western Antarctic Peninsula region, Ross, R. M., E. E. Hofmann and L. B. Quetin (editors), *Foundations for Ecological Research West of the Antarctic Peninsula.* American Geophysical Union, 1996.

Smith, R. C. and C. R. Booth, Oceanographic bio-optical profiling system, *A;;lied Optics*, *23*, 2791-2797, 1984.

Stammerjohn, S., and R. C. Smith, Spatial and temporal variability in West Antarctic sea ice coverage, Ross, R. M., E. E. Hofmann and L. B. Quetin (editors), *Foundations for Ecological Research West of the Antarctic Peninsula.* American Geophysical Union, 1996.

Stammerjohn S., and R. C. Smith, Opposing southern ocean climate patterns as revealed by trends in regional sea ice coverage, *Climate Change*, *37*, 617–638, 1997.

Stearns, C. R., and D. H. Bromwich, Sensible and latent heat flux estimates in Antarctica, Bromwich, D. H. and C. R. Stearns (editors), *Antarctic Meteorology and Climatology: Studies Based on Automatic Weather Stations*, volume *61*, 1993.

Steel, M. G., G. L. Mellor, and M. G. McPhee, The role of the molecular sublayer in the melting or freezing process, *J. Phys. Oceanogr.*, *19*, 139–147, 1989.

Stein, M., The distribution of water masses in the South Shetland Islands area during FIBEX, *Mem. Nat. Inst. Polar Res.*, *27*, 16–23, 1983.

Stein, M., Variability of water masses and currents off the Antarctic Peninsula during SIBEX, *Arch. FischWiss.*, *37*, 25–50, 1986.

Stein, M., Seasonal variation of waters masses in Bransfield Strait and adjacent waters, *Arch. FischWiss.*, *39*, 15–38, 1989.

Stein, M., Variability of local upwelling off the Antarctic Peninsula. 1986-1990, *Arch. FischWiss.*, *41*, 131–158, 1992.

Stein, M., and S. Rakusa-Suszczewski, Geostrophic currents in the South Shetland Islands area during FIBEX, *Mem. Nat. Inst. Polar Res.*, *27*, 24–34, 1983.

Stein, M., and S. Rakusa-Suszczewski, Meso-scale structure of water masses and bottom topography as the basis for krill distribution in the se Bransfield Strait February-March 1981, *Meeresforsch.*, *30*, 73–81, 1984.

Stossel, A., P. Lemke, and W. B. Owens, Coupled sea ice-mixed layer simulations for the Southern Ocean, *J. Geophys. Res.*, *95*, 9539–9555, 1990.

Turner, J. S., *Buoyancy Effects in Fluids*, Cambridge University, New York, 1973.

UNESCO, Algorithms for computation of fundamental properties of seawater, Fofonoff, N. P. and R. C. Millard, Jr. (editors), *Technical Papers in Marine Science.*, volume *44*, 53pp, 1983.

Van Loon H., A review of the surface climate of the Southern Hemisphere and some comparisons with the Northern Hemisphere, *J. of Marine Sys.*, *2*, 171–194, 1991.

Wamser, C. and D. G. Martinson, Drag coefficients for winter Antarctic pack ice, *J. Geophys. Res.*, *98*, 12,431–12,437, 1993.

Waters, K. J., and R. C. Smith, Palmer LTER: A sampling grid for the Palmer LTER program, *Antarctic J. of the U. S.*, *27*, 236–239, 1992.

Webb, D. J., P. D. Killworth, A. Coward, and S. Thompson, *The FRAM Atlas of the Southern Ocean.* Natural Environmental Research Council, Swindon, U.K., 1991.

White, W. B., and R. Peterson, An Antarctic circumpolar wave in surface pressure, wind, temperature, and sea-ice extent, *Nature*, *381*, 699–702, 1996.

Whitworth, T., III, W. D. Nowlin, Jr., A. H. Orsi, R. A. Locarnini, and S. G. Smith,

Weddell Sea shelf water in the Bransfield Strait and Weddell-Scotia Confluence, *Deep Sea Res.*, *41*, 629–641, 1994.

Zillerman, J. W., A study of some aspects of radiation and heat budgets of southern hemisphere oceans, *Meteorol. Stud.*, *26*, 562–575, 1972.

VITA

David A. Smith

Department of Ocean, Earth and Atmospheric Sciences
Old Dominion University
Norfolk, VA 23529

Education:

Ph.D. Ocean, Earth & Atmos. Sciences, Old Dominion University (1999)
B.A. Physics, West Virginia University (1990)
B.S. Secondary Education, West Virginia University (1990)

Professional Experience:

1991 - 1999	Graduate Research Assistant, Department of Oceanography, Old Dominion University, Norfolk VA
1990 - 1991	Graduate Teaching Assistant, Department of Physics, Old Dominion University, Norfolk VA

Publications:

Smith, D.A., E.E. Hofmann, J.K. Klinck and C.M. Lascara. Hydrography and circulation of the west Antarctic Peninsula continental shelf. *Deep-Sea Research*, 46: 925-949, 1999

Hofmann, E.E., J.M. Klinck, C.M. Lascara and D.A. Smith. Water mass distribution and circulation west of the Antarctic Peninsula. In: *Foundations for ecological research west of the Antarctic Peninsula*, Ross, R.M., E.E. Hofmann and L.B. Quetin, editors, Antarctic Research Series, Vol. 70, American Geophysical Union, Washington DC., pp 61-80, 1996.

Klinck, J.M. and D.A. Smith. Effect of wind changes during the last glacial maximum on the circulation in the Southern Ocean. *Paleoceanography*, 8: 427-433, 1993.